WHOI-2002-01

Woods Hole Oceanographic Institution

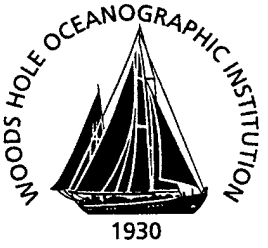

Shearmeter Floats in the Area of the WHOI Brazil Basin Tracer Release Experiment: Technical and Oceanographic Data

by

Timothy F. Duda
Brian J. Guest
Christine M. Wooding
Clayton M. Jones
Scott Lelievre
Douglas C. Webb

Woods Hole Oceanographic Institution
Woods Hole, Massachusetts 02543

January 2002

Technical Report

Funding was provided by the National Science Foundation under Grant Nos. OCE-9416014 and OCE-9906685.

WHOI-2002-01

Shearmeter Floats in the Area of the WHOI Brazil Basin Tracer Release Experiment: Technical and Oceanographic Data

by

Timothy F. Duda
Brian J. Guest
Christine M. Wooding
Clayton M. Jones
Scott Lelievre
Douglas C. Webb

January 2002

Technical Report

Funding was provided by the National Science Foundation under Grant Nos. OCE-9416014 and OCE-9906685.

Approved for Distribution:

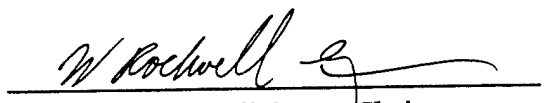

W. Rockwell Geyer, Chair

Department of Applied Ocean Physics and Engineering

Shearmeter Floats in the Area of the WHOI Brazil Basin Tracer Release Experiment: Technical and Oceanographic Data

Timothy F. Duda, Brian J. Guest, Christine M. Wooding

Woods Hole Oceanographic Institution
Woods Hole, MA, 01543

Clayton M. Jones, Scott Lelievre, and Douglas C. Webb

Webb Research Corporation
East Falmouth, MA 02536

Abstract

Six drifting floats designed to measure shear were deployed in the vicinity of the Brazil Basin Tracer Release Experiment. The one-year long time series of oceanographic conditions obtained by the floats are for direct comparison with long-term tracer dispersion. The purpose of the tracer dispersion experiment was to study mixing of Antarctic Bottom Water at approximately 4000 m depth with less dense water above. Two of the floats returned shear records, one from about 1660 m depth and one from about 2800 m depth. Mean shear at 1660 m was $2.2 \times 10^{-3}\ s^{-1}$ *with N = 1.1 cph, about 1.9 times the Garrett-Munk model amount. Mean shear at 2800 m was* 1.1×10^{-3} *with N = 0.5 cph, about 2.2 times Garrett-Munk. There was no apparent depth structure to the shear recorded by the near-bottom float moving over the mountainous seafloor. The two shear time series and the local tidal velocities were not strongly correlated, but the tide and shear series did have some similarities. Some variability in the 1660-m shear may be due to atmospheric forcing. Three floats deeper than 2800 m returned one-year long trajectories. Two trajectories were persistently eastward.*

Table of Contents

1. Introduction

The multi-investigator Brazil Basin Tracer Release Experiment (BBTRE) centered around the release and tracking of the chemical sulfur hexafluoride by Dr. James Ledwell and associates from the Applied Ocean Physics and Engineering (AOPE) Department of the Woods Hole Oceanographic Institution (WHOI). Four additional components were fine and microstructure profiling by Drs. Ray Schmitt, John Toole and Kurt Polzin of the WHOI Physical Oceanography (PO) Department, a SeaBeam bathymetric study by Peter Lemmond of the WHOI Geology and Geophysics Department, a mooring deployment by the WHOI PO Dept., and this shearmeter float effort. The goals of the project were to quantify tracer dispersal at the top of the Antarctic Bottom Water layer, at roughly 4000 m depth, and to identify the responsible mechanisms.

One prototype shearmeter was deployed in March 1998 at the BBTRE site as the final task of the WHOI AOPE shearmeter NSF development project. The float was launched from the *RV Seward Johnson* by Brian Guest. That instrument operated as intended for 100 days. Subsequently, six shearmeters were built as a component of the BBTRE program itself and taken to the site in early 2000 aboard the *RV Knorr*. Five were deployed. These were the first production model shearmeters from Webb Research Corporation. The two designs differed in that the prototype was limited to the upper two kilometers of the water column, whereas the production units were capable of operating at the SF_6 depth of 4000 m.

2. Design and Construction

The shearmeters are drifting spar-buoy shaped floats. They have vanes at either end, which cause the entire float to rotate in response to currents at the ends. The vanes are similar to anemometer vanes. In a vertically invariant current the flow will be zero at each end, resulting in no rotation, whereas in a sheared flow the current will not be zero at the ends, but will be approximately equal and opposite, resulting in rotation. The vanes measure the magnitude of the flow, thus making the flow directions irrelevant, but also undetectable via this method. The above description of how the floats work disregards the effects of vertical currents on these quasi-isobaric floats. (The floats will respond to oscillatory isopycnal displacements by heaving, in phase, with amplitude less than the isotherm displacement ($1/10^{th}$ to $1/3^{rd}$), see *e.g. Goodman and Levine* (1990).) A modification to allow tilt and to measure its direction, thus measuring shear direction, was not undertaken.

Two configurations were used in the BBTRE, prototype and production. They had construction and sensor differences. Most fundamentally, the prototype was tapered, with narrow upper and lower sections, and it measured only pressure, temperature, and rotation. The production units were not tapered and measured two additional quantities: RAFOS acoustic tracking signals and temperature difference between the two float ends. The temperature difference system used two thermistors and was independent of the absolute temperature circuit. All shearmeters used modular RAFOS-float controllers and battery packs provided by Seascan, Inc. of Falmouth, Massachusetts. Druck pressure sensors and aged thermistors were used.

Other details of the prototype are described here. It is shown in Figures 2-1 and 2-2. It had three end-to-end sections. The center section was an 18 ft (5.48 m) long, 3-inch outside diameter (OD), 0.25-inch wall 6061 alloy aluminum tube, not anodized. At each end were 6-ft (1.83 m) hard-anodized sections scaled down by half to 1.5-inch OD, 0.125-inch wall thickness. All sections had the same strength against isotropic crushing pressure force. The vanes were at the ends, separated by 9.2 m, Figure 2-2. The prototype, made of 6061 material, was not capable of withstanding pressures at the dye depth. It was ballasted to drift at 1500 m depth.

The production models, one of which is shown in Figure 2-3, were of hard-anodized and epoxy-painted 7075 alloy tubing having 0.25-inch wall thickness and 3.25-inch outside diameter. Each float had three 124-inch tubing sections. The sections were mated with machined and anodized 6061-T6 cylindrical coupling sleeves to form a single long pressure case. The sleeves and end caps were

assembled to the tubes with stainless-steel V-band clamps. Each joint had a piston-type O-ring seal with a backing ring (Figure 2-4).

The rotation-inducing vanes (Figures 2-1, 2-2 and 2-3), each consisting of a spindle (Figure 2-5) and a 5-inch (12.7 cm) diameter cup (Figure 2-6), all of hard-anodized aluminum alloy, were essentially identical on all floats. Each spindle is attached to the side of a cup, eliminating lift from the vertical component of flow that would result from bumps on the backs of the cup (an early design oversight). Six vanes were mounted at uniform azimuthal increments at each end. The distance from the center axis of a float to the outboard edges of the vane assemblies was 45 cm, giving a diameter of 90 cm.

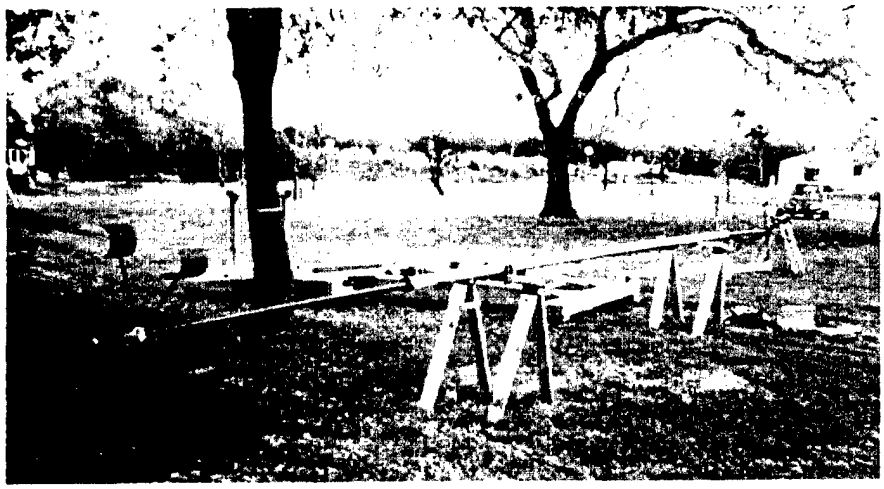

Figure 2-1. Prototype Shearmeter.

3. Ballasting

All instruments were ballasted in Great Harbor, Woods Hole, in the large well of the WHOI Pier at slack tides on the dates listed in Table 3-1. Winter seemed like an advantageous time because the harbor temperature was near the temperature at the desired deployment depth, so any error in the thermal expansion coefficient on the alloy would not result in a ballasting error. Alas, the temperature coefficient is better known than the other pertinent float parameter, the bulk compressibility of the float, which is dependent on geometrical configuration, so the benefit of winter was in reality nil. The harbor water temperature over the depth range of the floats was measured with an SBE39 temperature/pressure sensor. The salinity was estimated from the conductivity of bottle samples, which was measured with a benchtop Guildline Autosal instrument by Mr. George Tupper of the PO Dept. The displacement of the floats under the ballasting conditions can be computed if they are neutrally buoyant. The desired displacement of the floats under deployment conditions can also be computed. Using these quantities, the necessary amount of internal deployment ballast mass M_I is given by

$$M_I = 0.87 M_S + \Delta M$$

where M_S is exterior steel hardware hung on the float to achieve neutral buoyancy, and where ΔM is the amount of mass that must be added to the ballast configuration to achieve neutral buoyancy

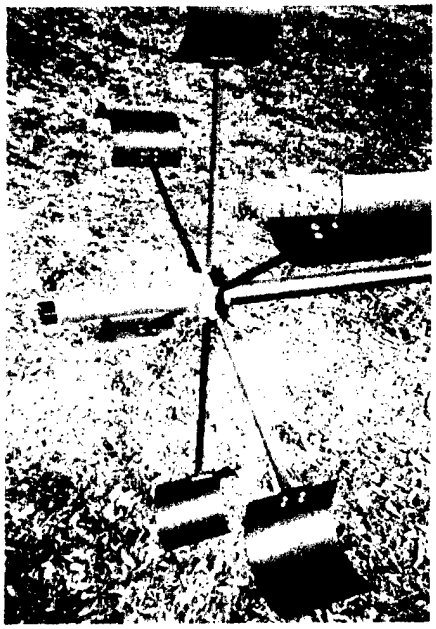

Figure 2-2. Detail of prototype vanes. The axial tube contains the drop weight.

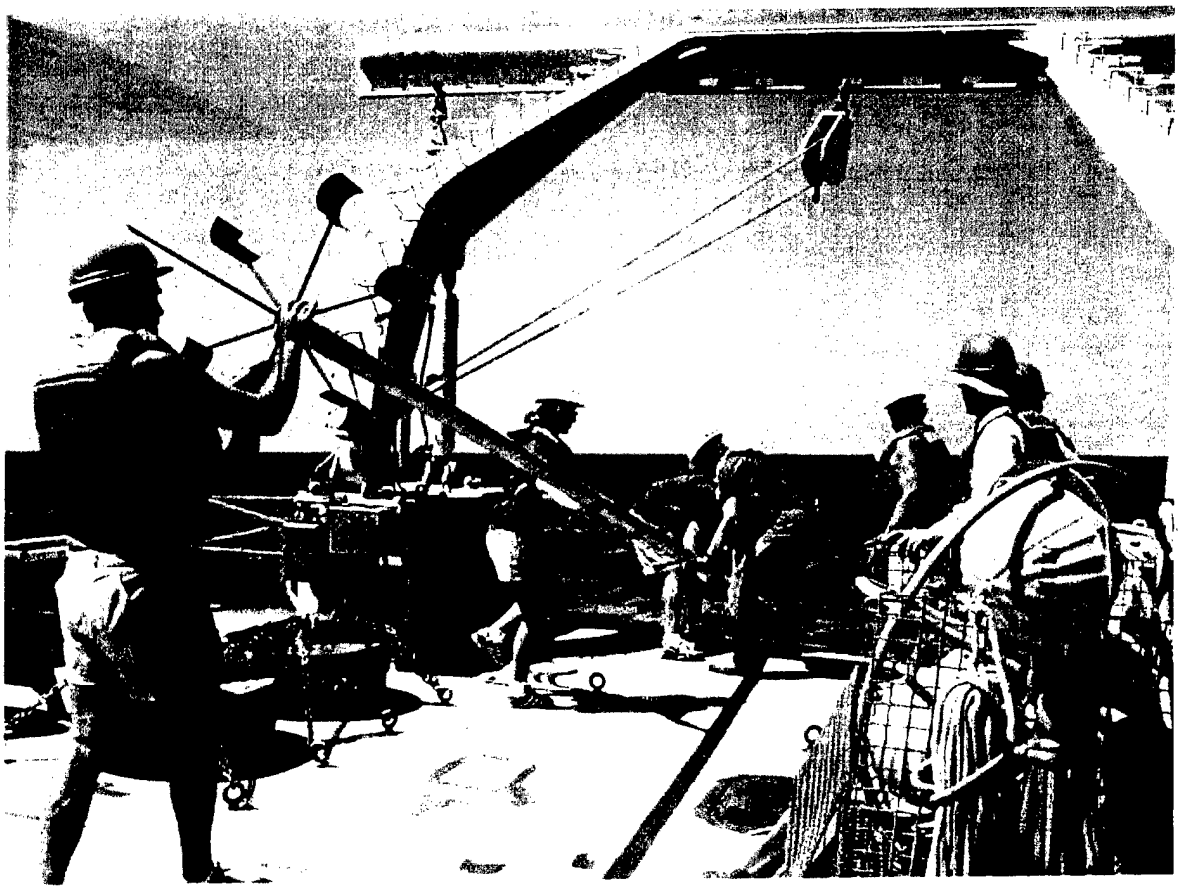

Figure 2-3. A production shearmeter being launched from the *RV Oceanus* in February 2001, east of Barbados. This float has two tubing sections; the BBTRE floats had three.

under deployment conditions at sea. The mass ΔM can be computed using the expression for deployment density (mass per unit volume), which is

$$\rho_D = \frac{M_B + \Delta M}{\frac{M_B}{\rho_B}(1 + \alpha\Delta P + \beta\Delta T)}$$

The subscripts B indicate ballast conditions, subscripts D indicate deployment conditions, α is the fractional compression per decibar of the floats, estimated to be $\alpha = -1.6 \times 10^{-6}$, β is the fractional thermal expansion per degree for aluminum, which is $\beta = 7 \times 10^{-5}$, M_B is float mass during ballasting, and ρ_D is float density during deployment (equal to *in situ* water ocean density). Finally, $\Delta P = P_D - P_B$ and $\Delta T = T_D - T_B$. Note that this α value means that the relative compressibility with respect to seawater is $s = 0.4$ in the notation used by *Goodman and Levine* (1990).

During ballasting, the temperature varied by roughly 0.01 °C rms over the 10-m instrument span and over the time necessary to ballast. For all floats, density and temperature vs. depth in the area taken from Ledwell's CTD station 22 of the previous BBTRE cruise. Ballasting information is shown in Table 3-1. A mass of 15 grams was deleted from year-2000 floats because the prototype settled too deep, but this is not indicated in the table. This could be added to the first equation as a "fudge factor".

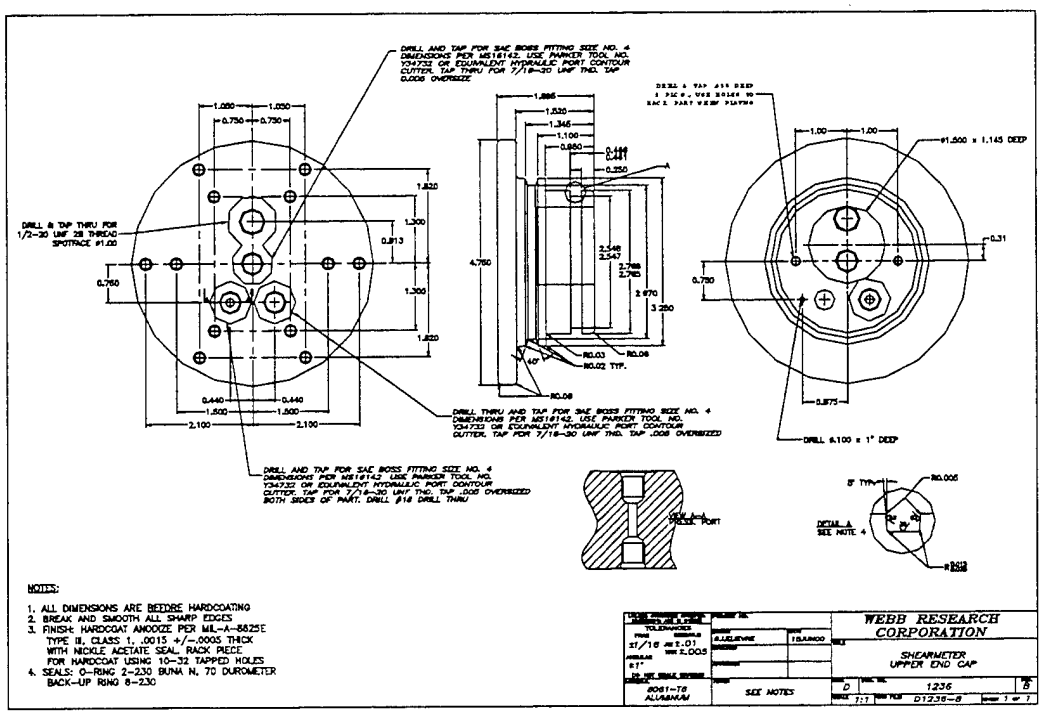

Figure 2-4. Diagram of the production model upper end cap is shown. Bolted to the outside are six vane spokes, an antenna, and a hydrophone. Bolted to the inside are a pressure sensor and an electronics chassis.

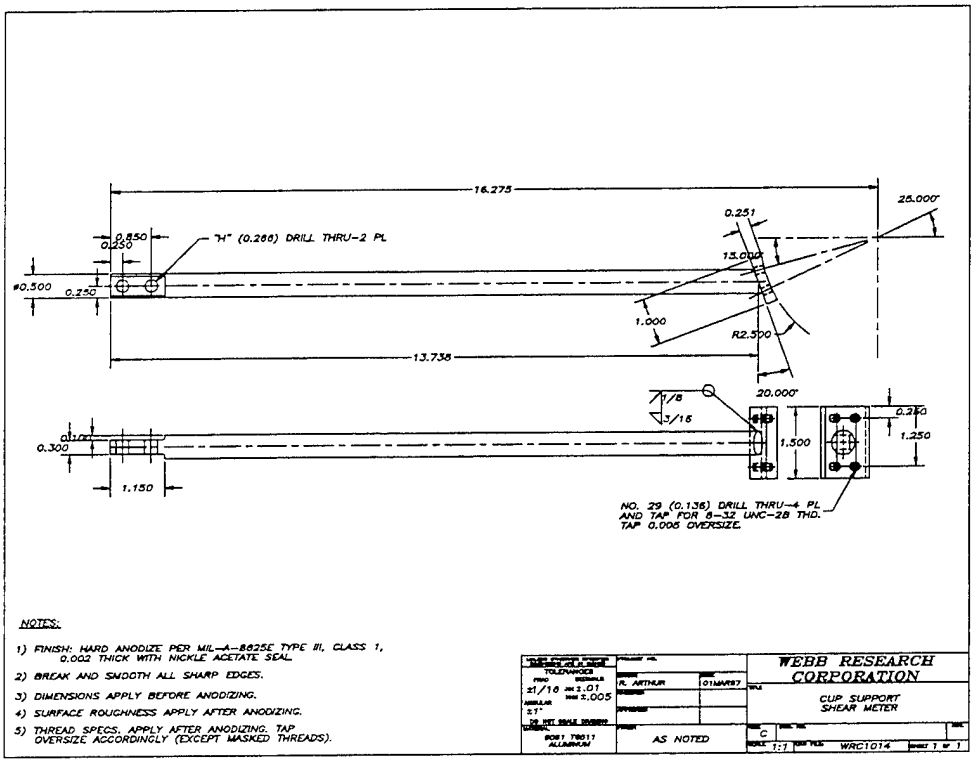

Figure 2-5. Diagram of one vane spoke. To prevent deformation from welding, the tab is welded to the spoke before the 2.5-inch radius curve is cut.

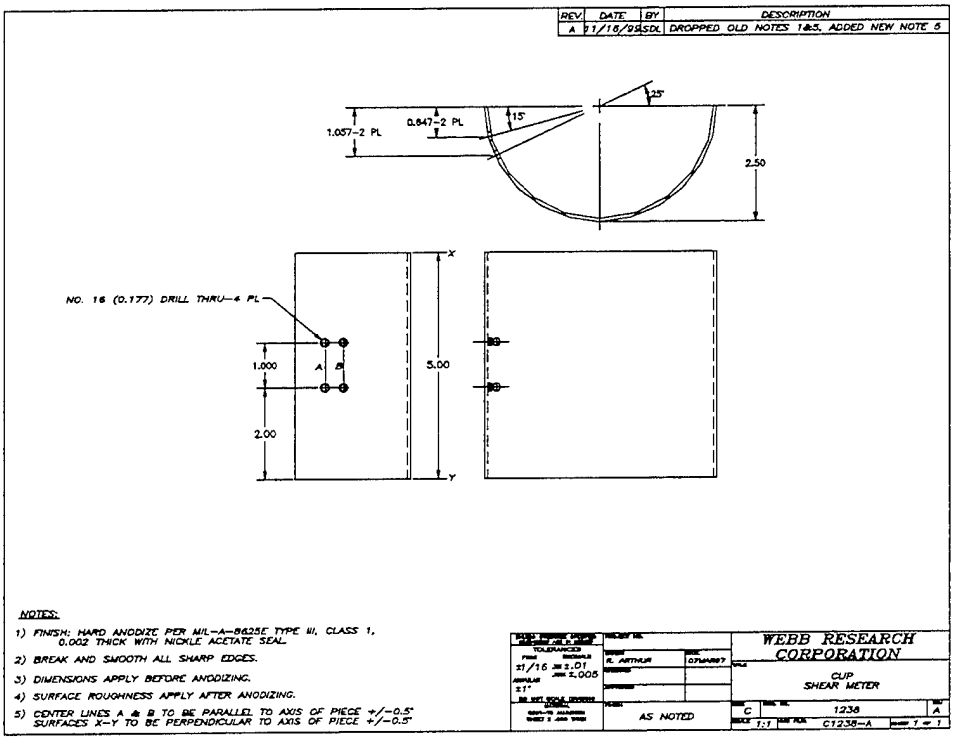

Figure 2-6. The current-sensing cup that is bolted to a spoke, one of twelve per float.

Table 3-1. Ballasting (B) and deployment (D) parameters. Pressure in decibars, mass in kg.

SN	Date	S_B psu	T_B °C	P_B	ρ_D kg/m^3	T_D °C	P_D	M_B	M_S	M_I
001	1/28/98	31.176	2.900	5	1034.57	3.546	1500	34.18	0.644	0.800
099	3/01/00	32.176	2.863	5	1045.91	1.726	4000	54.617	0.261	0.947
100	2/25/00	32.285	1.801	5	1041.46	2.685	3000	54.685	0.275	0.812
101	2/29/00	32.180	2.644	5	1043.69	2.266	3500	54.502	0.288	0.898
102	2/29/00	32.180	2.644	5	1043.69	2.266	3500	54.601	0.277	0.890
103	3/01/00	32.176	2.863	5	1045.91	1.726	4000	54.594	0.300	0.982
104	3/01/00	32.176	2.863	5	1045.91	1.726	4000	54.708	0.242	0.932

4. RAFOS Sources, Float Deployment and Data Recovery

In all, six floats were deployed in the region of the SF_6 tracer plume. The prototype float was deployed in March 1998. It was trucked to Florida by Webb Research, prepared there by Dan Webb, and deployed by Brian Guest. Five high-strength alloy production shearmeters were launched in May 2000. One other float (SN 103) was damaged at deployment time in 2000. After assembly and ballasting, the floats had been flown to Ponta Delgada in the Azores for final assembly aboard the *RV Knorr* (thus the 3-tube design, allowing six floats to fit inside a 118 by 70 by 30 inch wooden crate). The ship then transited to Recife, Brazil, where the BBTRE scientific party boarded, finally proceeding to the BBTRE site. Four of the year-2000 floats were programmed to collect data for one year, and one was programmed for a short mission of 6 months. The short mission provided a check of float design and functionality before assembly of a second batch of floats, to be deployed in the North Atlantic in February 2001.

When assembling the floats, the O-rings areas were covered with large quantities of petroleum-based Parker O-Lube. The idea was to completely fill the gap between the end caps and the tubing to prevent crevice-corrosion of the susceptible 7075-alloy tubing. The unfinished exterior clamps were covered with green waterproof wheel-bearing grease.

Between November 1994 and February 2000, twenty-one RAFOS-system sound sources were deployed in the South Atlantic. Of these, five were probable candidates to be heard by the shearmeters. These were named **B6**, **B7**, **53N**, **M11** and **M12**, with the first three also known as **27**, **28**, and **6**. **53N** is additionally known as **198**. Their positions are shown in Figure 4-1. Sources **M12** and **B7** transmitted in the 0100 UTC window, while **M11**, **B6** and **53N** transmitted in the 0130 UTC window, all daily. **53N** transmitted 35 s early.

Sources **B6** and **B7** were deployed from the *RV Knorr* on the year 2000 BBTRE SF_6 sampling and shearmeter deployment cruise. The **B6** position is 10° S, 24.982° W; the **B7** position is 23.883° S, 25.255° W. Sources **M11** and **M12** were deployed on 16 and 20 September, 1997, respectively, at positions 29.986° S, 5.978° W and 20.01° S, 6.024° W. Source **53N** was deployed on 16 March 1995 at 19.737° S, 22.713° W. Distances from the Brazil Basin sources **B6**, **B7** and **53N** to the position 21.8° S, 18.3° W, a nominal deployment position, were 1488, 750 and 513 km respectively, corresponding to 993, 500 and 342 s travel times at the locally depth-integrated sound channel speed of 1498.5 m/s, obtained from BBTRE CTD data.

Tables 4-1 and 4-2 show shearmeter mission parameters. The prototype floated deeper than anticipated. The later units floated shallower than anticipated. One float failed to transmit data. Its degree of functionality is unknown. The direction of travel for the floats ranged from northeast to

south, and the speeds ranged from 0.3 to 1.3 cm/s. The trajectories of three floats are discussed in a later section.

The prototype float transmitted 32-byte long data packets through the System ARGOS satellites. Float 001 transmitted packets at 90-s intervals, the later floats at 45-second intervals (randomized in timing about this nominal interval, as requested by ARGOS). Figure 4-2 shows percentage of data returned, ratio of repeat to new packets, and number of new data packets per day, as functions of time, for float SN 001. For all floats, packets were divided into 10 interleaved groups of packets. The packets in each group are sequentially transmitted, group after group, until all data have been transmitted. Then the pattern is repeated.

Table 4-1. Deployment information.

SN	Deploy Lat. S	Deploy Long. W	Surface Lat. S	Surface Long. W	Target depth (m)	Actual depth (m)
001	21° 36.79	17° 42.19	21° 02.28	16° 40.98	1500	1660
099	21° 42.64	18° 37.93	20° 59.58	18° 06.66	4000	3550
100	21° 50.03	18° 18.50	23° 27.18	14° 46.98	3000	2800
101	21° 50.03	18° 18.50	21° 55.50	16° 30.00	3500	3130
102	21° 51.36	18° 35.22	23° 42.60	19° 05.94	3500	3500
103	--	--	--	--	--	--
104	21 42.65	18 37.84	--	--	4000	--

Surface: First position fix, which may be after initial reception of data packets.

Table 4-2. Additional deployment information.

SN	ARGOS PTT	Deployment Time	Surface Time	Days	Distance (km)	Speed (cm/s)	Course
001	01942	26 Mar 98 1000	5 July 98 0149	100	123.5	1.43	59.2°
099	01943	7 May 00 0514	7 May 01 0320	365	96.1	0.30	34.3°
100	22632	6 May 00 1005	7 May 01 2213	365	404.3	1.28	117.0°
101	22633	6 May 00 1020	1 Nov 00 0335	179	187.2	1.19	93.4°
102	22634	6 May 00 0755	7 May 01 2032	365	211.9	0.67	194.3°
103	22635	--	--	--	--	--	--
104	22636	7 May 00 0519	No signal	365	--	--	--

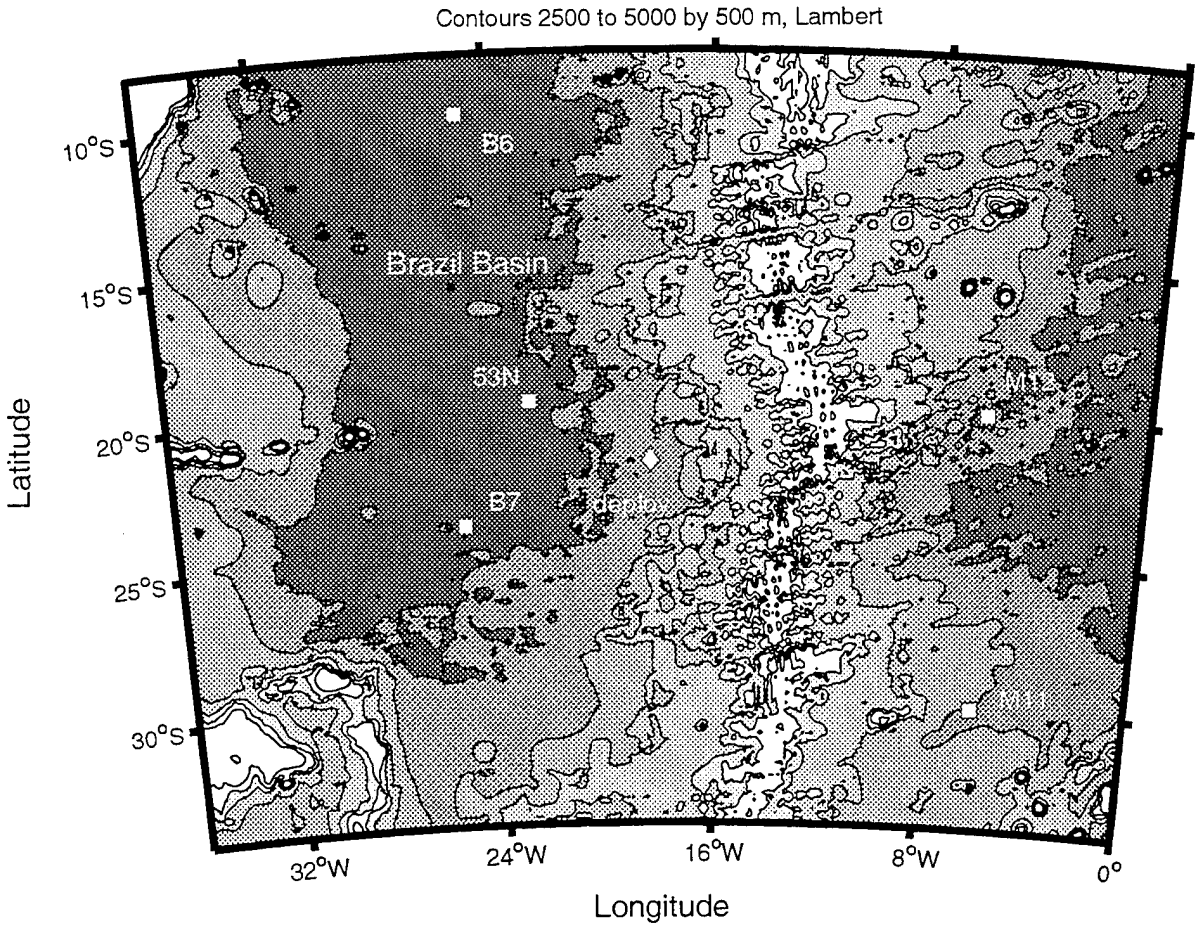

Figure 4-1. Five RAFOS-system sound sources were available in the deployment area

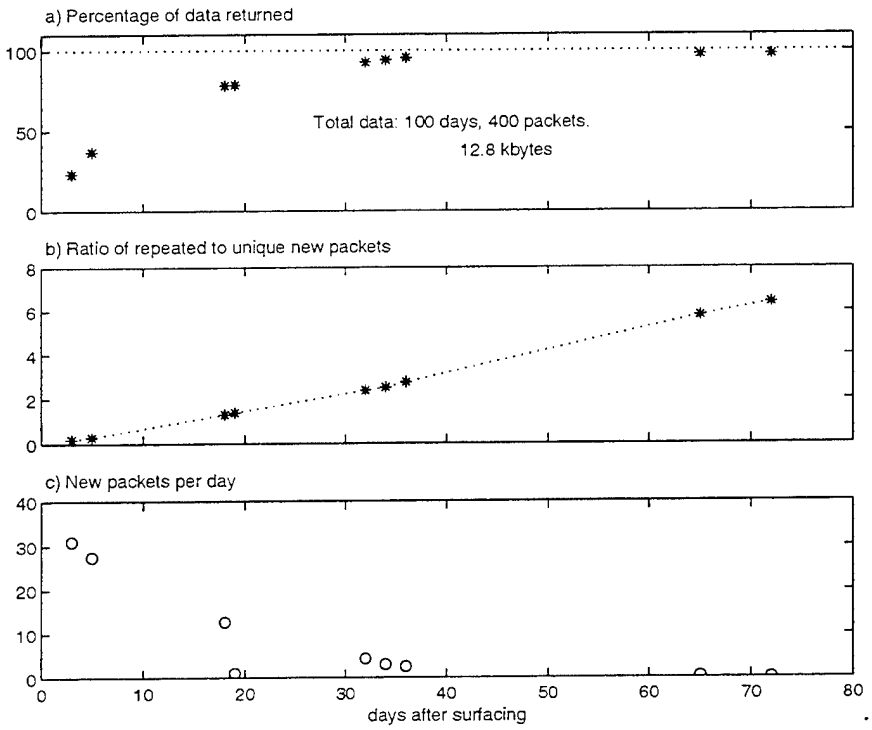

Figure 4-2. a) The percentage of the 400 data packets from the prototype float retrieved through System ARGOS is shown after each of nine intervals. 92.5% of the data were retrieved after 32 days (370 of 400 packets). 389 packets were recovered after 65 days. b) The cumulative ratio of repeated to unique packets is shown, also computed after each interval. c) The average number of new packets received per day is shown for each interval.

5. Float System Performance

The prototype float functioned flawlessly. However, not all of the five year-2000 floats which provided data were fully functional. The parts for those floats were barely collected together before they needed to be shipped to meet the final research vessel scheduled to work in the BBTRE area in the foreseeable future. This was largely due to a delay in the manufacture of the 7075 tubing at a mill in the UK. As a consequence, the floats were not tested in the assembled state, although all electronic components had been tested individually.

Table 5-1 shows the performance of the floats at sea. No information is available for float 104, which sent no data. It is not known whether it leaked, had a controller hardware failure, had an ARGOS hardware failure, or suffered from a programming error. There were four known system failures in the other floats: three rotation-sensing compass systems failed altogether, and one RAFOS listening system failed to detect any sources after 15 days.

The rotation-sensing system used a two-axis magnetometer to detect the compass octant (sector) of the float heading. The sensor was mounted close to the upper end-cap. The float heading was checked one per second. Change to a new sector incremented or decremented a counter. The counter value was written to data-packet memory once per hour. Due to the fact that the rotation systems and programs worked on the bench, the failures were apparently due to the proximity of the Druck pressure sensor to the magnetometers, or to the proximity of the stainless steel clamp fastening the end cap and tube. The temperature difference (ΔT) measurement between the two ends drifted across its

full-scale range (2.048 degrees, with resolution of 0.5 mdeg) in three instruments. The drift is very slow and can be filtered out, however, to obtain temperature gradient over the scale of the floats, thereby also giving density gradient, which can be combined with shear to obtain gradient Richardson number. The ΔT noise level is not known. All data are shown in the next section.

Table 5-1. Float sensor and system functionality at sea. Dash means not equipped.

SN / ID	P	T	ΔT	Rotation	RAFOS	ARGOS
001 / 01942	ok	ok	--	ok	--	ok
099 / 01943	ok	ok	**drift**	**fail**	ok	ok
100 / 22632	ok	ok	**drift**	ok	ok	ok
101 / 22633	ok	ok	ok	**fail**	ok	ok
102 / 22634	ok	ok	**drift**	**fail**	**fail**	ok
104 / 22636	?	?	?	?	?	?

6. Oceanographic Data

6.1. Plots of Basic Data

Here we show plots of the unprocessed data from the five functional floats in Figures 6-1 through 6-9. The first figure shows hourly pressure *(P)*, temperature *(T)* and rotation *(R)* from float 001, its only data. The next eight figures are in pairs, showing first the hourly *R* data and the four-times daily *P* and *T* data for each year-2000 float, then the times of the highest peak of the RAFOS-system acoustic signal correlation processing, in the 0100 and 0130 UTC windows, again for each float. Data were collected on a six-hour cycle. RAFOS, *P* and *T* data were collected near the beginning of each cycle, while *R* and delta-*T* data were collected hourly. Data from ARGOS packets received before 19 November 2001 are included for the year 2000 floats; all data are included for the 1998 float.

Figures 6-1, 6-2, 6-4, 6-6 and 6-8 show that all floats sank gradually over time, although at differing rates. The temperatures fluctuated roughly 50 millidegrees at high frequency, and changed by up to 0.3 degrees over the long term. The rotation counter decremented properly in two floats, SN 001 and SN 100 (Figures 6-1 and 6-4). Figure 6-4 shows a few rotation counter data errors and *P* errors despite removal of packets with incorrect checksums. Float 099 moved into cooler water as it descended (Figure 6-2). Float 100 initially descended with no temperature change but then moved into cooler water over the last three months. Float 101 recorded more high-frequency temperature variability than the other floats (either signal or noise) and sank into only slightly cooler water. Float 102 moved through water of variable temperatures ranging from 1.8 to 2.2 degrees.

Figures 6-3, 6-5, 6-7 and 6-9 show the arrival times of the largest RAFOS signal correlation peak in each 0100 and 0130 UTC data window. The amplitudes and times of the two largest peaks in each window were recorded daily, but only the times of the largest peaks in each window are shown. The figures indicate that signals from sources **B6**, **B7** and **53N** were received. Figure 6-5 shows that float 100, which drifted 404 km eastward, also heard source **M12** in the 0100 window. Figure 6-10 shows the times for the largest RAFOS arrivals in the two windows commencing at 1300 and 1330 UTC for three floats. Float 099 did not detect any signals, but floats 100 and 101 both detected signals with closing range, presumably from **M11** and **M12**. The **M11** and **M12** signals were not used for tracking.

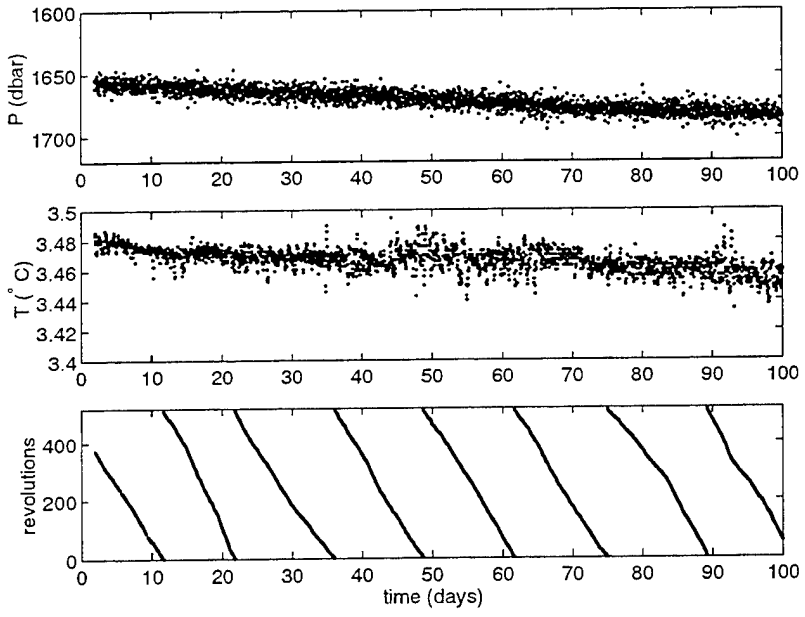

Figure 6-1. Oceanographic data from the prototype float, SN 001.

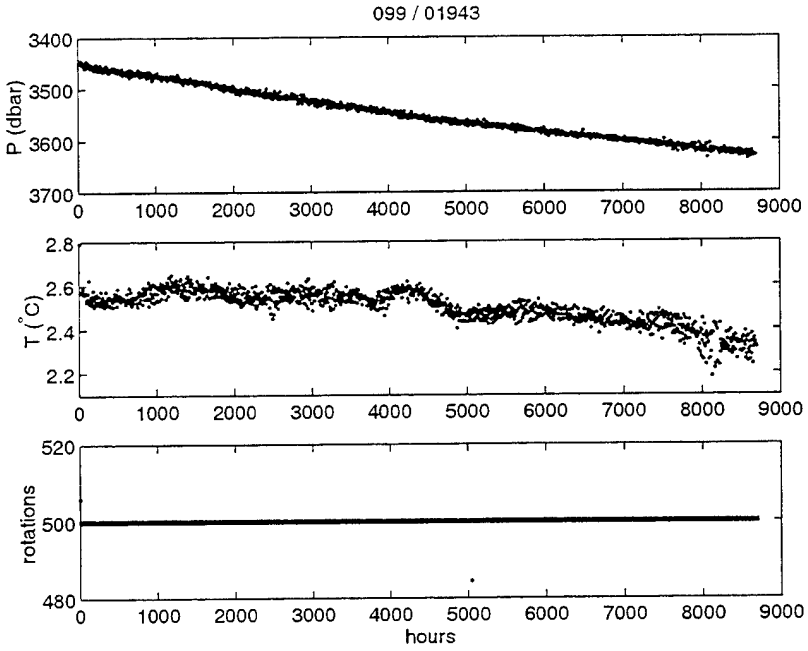

Figure 6-2. Fundamental oceanographic data from float 099.

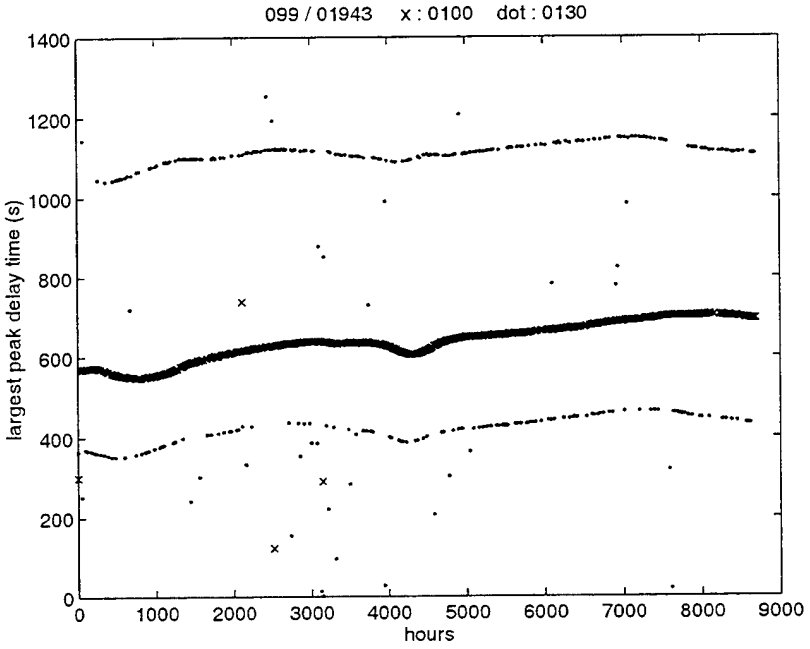

Figure 6-3. Arrival times of RAFOS signal peaks in the 0100 and UTC windows, float 099. The maximum peak in each window is shown.

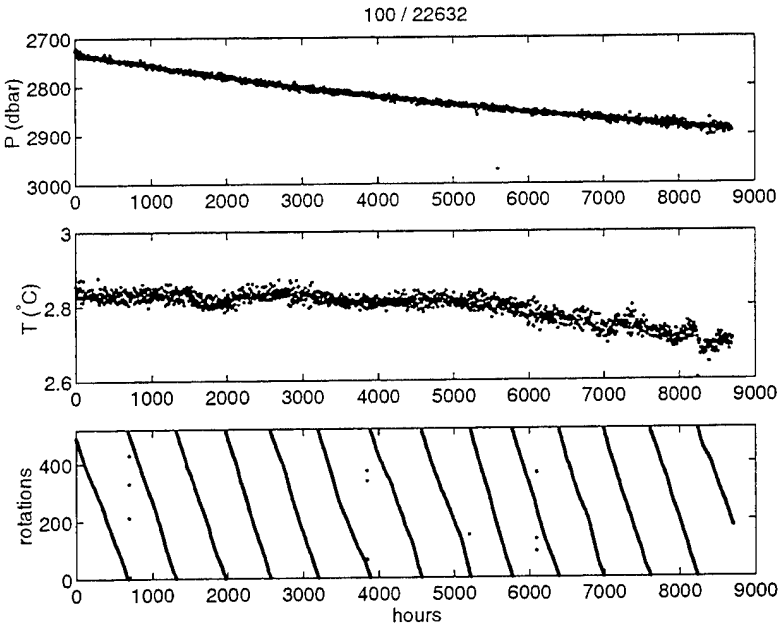

Figure 6-4. Fundamental oceanographic data from float 100.

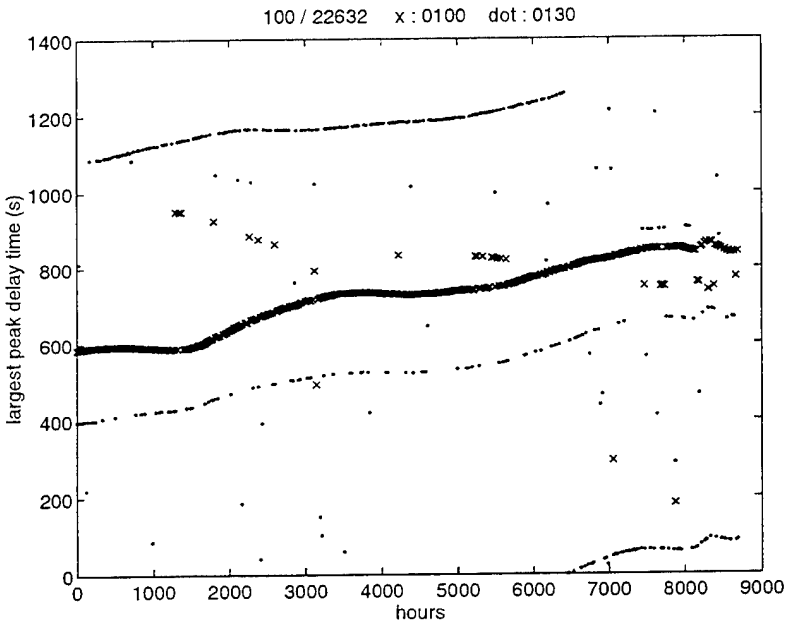

Figure 6-5. Arrival times of RAFOS signal peaks in the 0100 and 0130 windows, float 100. The loudest peak in each window is shown.

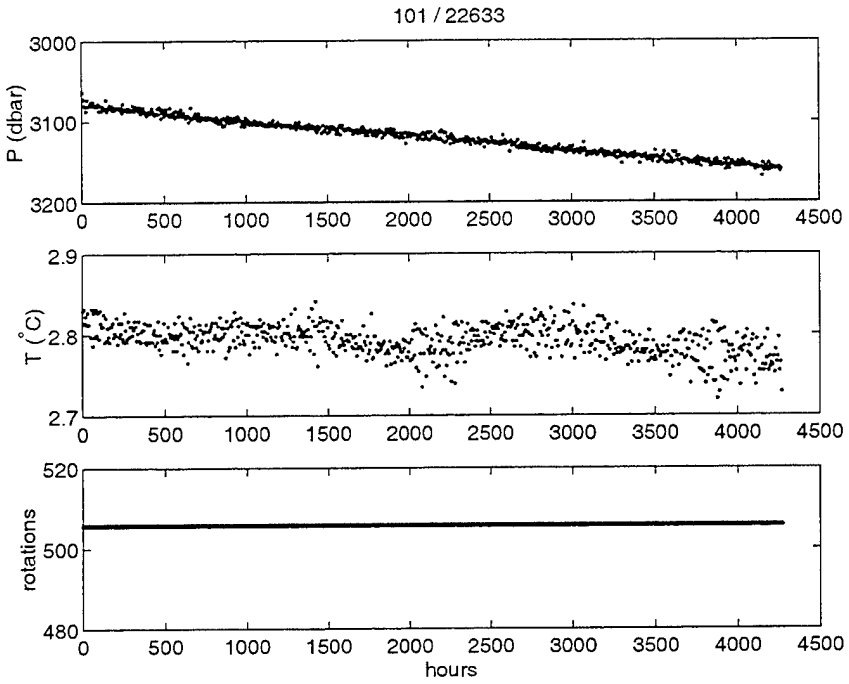

Figure 6-6. Oceanographic data from float 101.

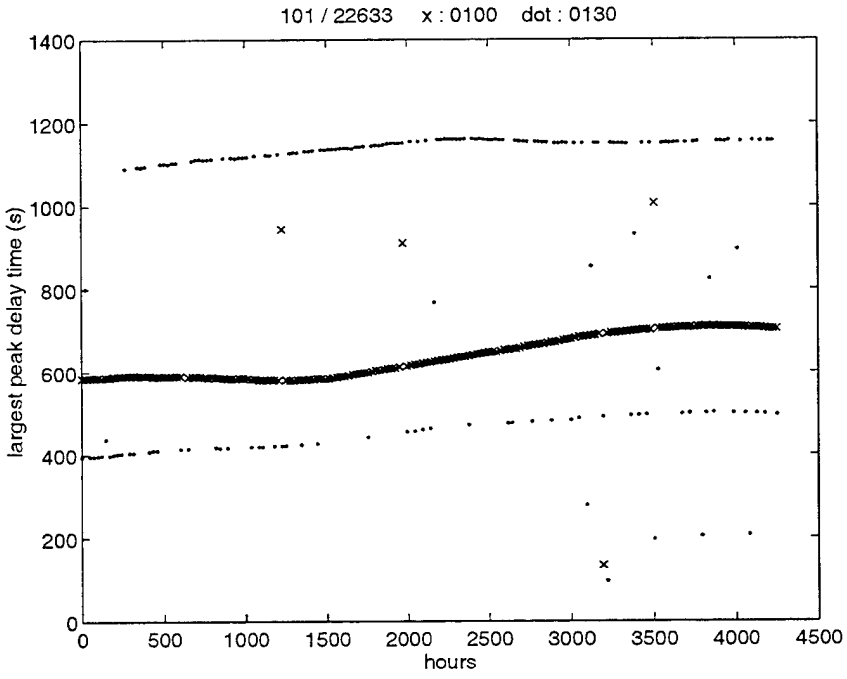

Figure 6-7. Arrival times of RAFOS signals in the 0100 and 0130 windows, float 101. The largest peak in each window is shown.

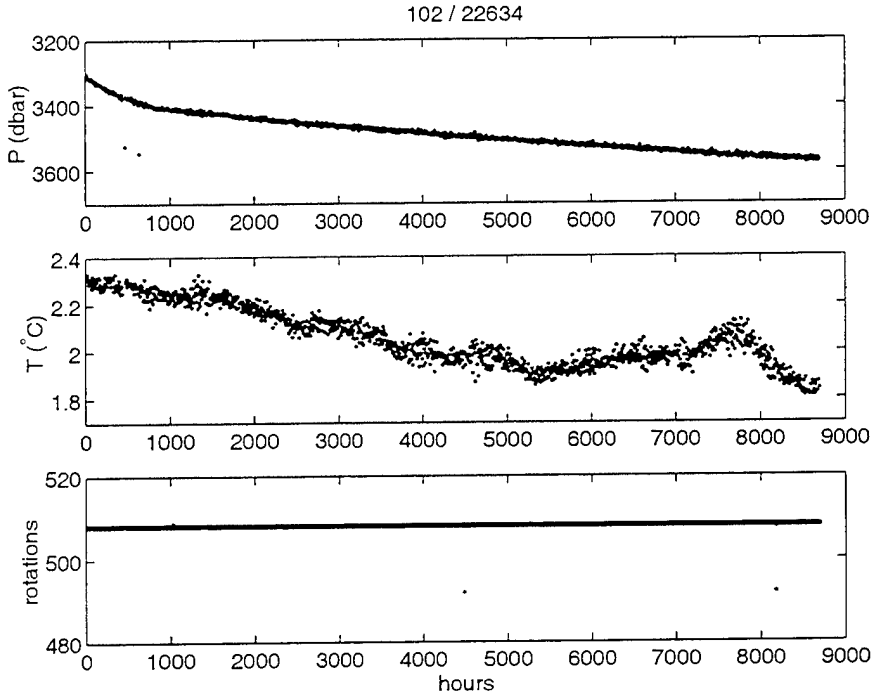

Figure 6-8. Oceanographic data from float 102.

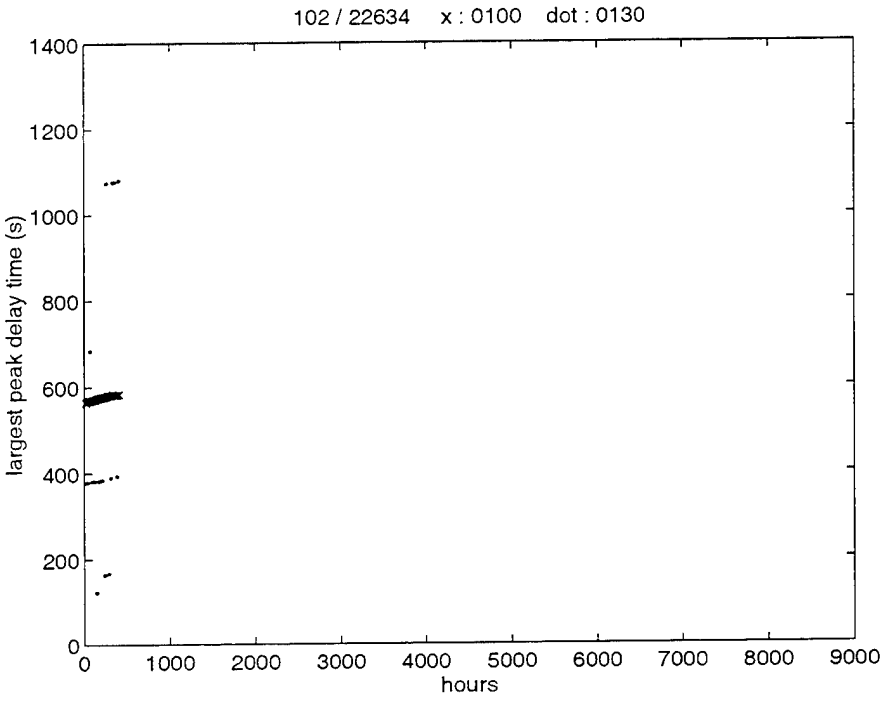

Figure 6-9: UTC 0100 and 0130 RAFOS signals for float 102 are usable for only 400 hours. The largest peak in each window is shown.

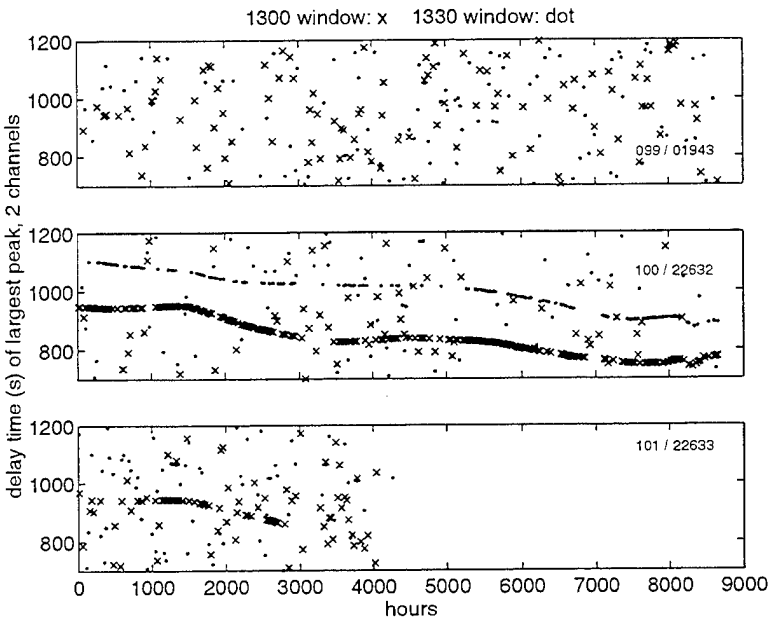

Figure 6-10. 1300 and 1330 UTC RAFOS arrivals for three floats. The times of the largest peak in each daily window are plotted.

6.2. Year 2000 Float Tracks

Floats 099, 100 and 101 were tracked for the duration of their missions. One additional float, 102, was tracked for 15 days. Figure 6-11 shows the tracks superimposed on *Smith and Sandwell* (1997) bathymetry. The surfacing positions are also plotted. The tracks for the first 16 days are plotted in Figure 6-12. The four tracks begin about 8 km to the east of the deployment positions, indicating a bias in the tracking procedure as implemented.

The mean zonal and meridional velocities are given in Table 6-1, as are the rms fluctuation velocities of the daily trajectory points about the mean. Figure 6-13 shows the tracks in units of east and north distance from their initial positions, with distance computed from the trajectory latitudes and longitudes using the WGS 1984 earth ellipsoid. The movement of two of the floats at over 1 cm/s to the east does not agree well with the inverse-modeled flow of *St. Laurent, Toole and Schmitt* (2001, Figures 5 and 6).

Figures 6-14 and 6-15 show that the float velocities are close to normal. In these plots of the distributions, the vertical axes have been adjusted such that normal data would fall on a line. These statistics can be compared to those of *Bracco, LaCasce and Provenzale* (2000), for example. They measured approximately normal distributions for small velocities such as these.

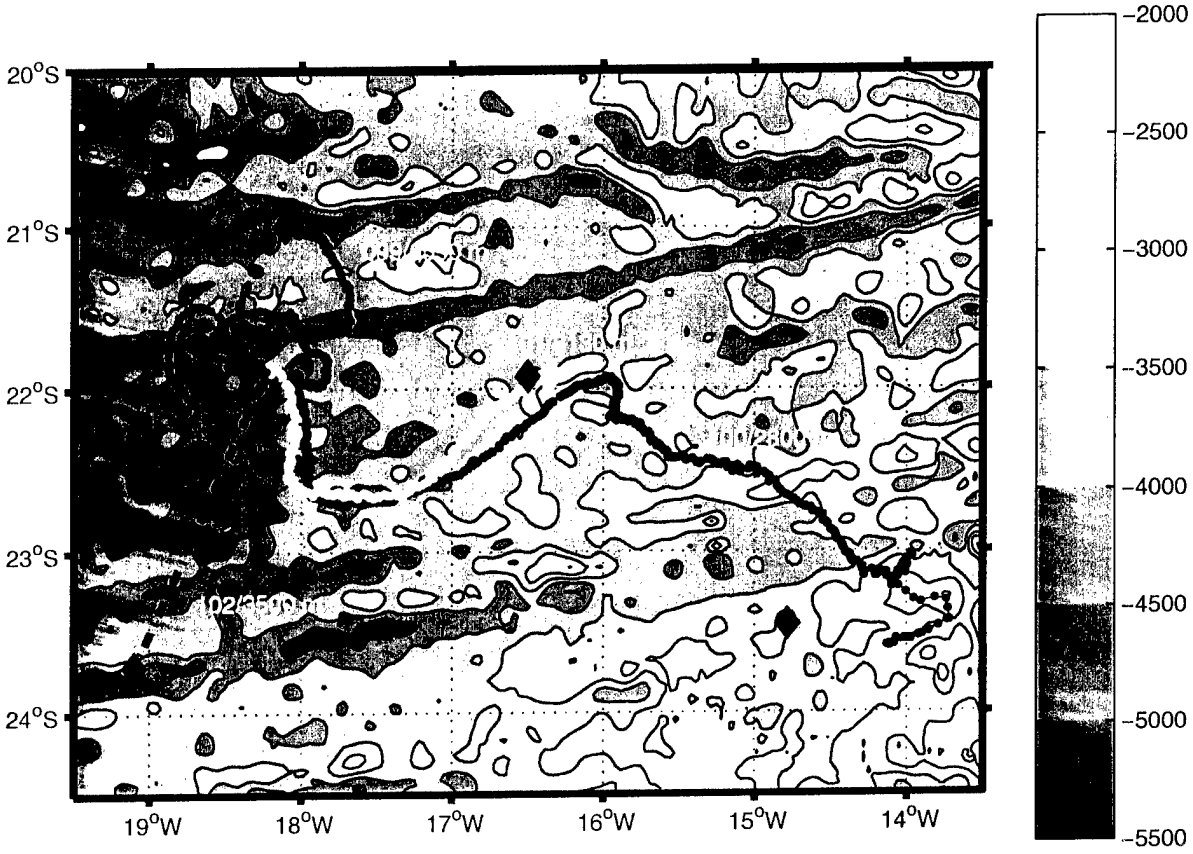

Figure 6-11. The four float trajectories are shown. The recovery locations are shown with red diamonds. The labels show the float SN and average depth. Float SN 102 was tracked for only 16 days; its short trajectory is connected to its recovery location with a dot-dash line.

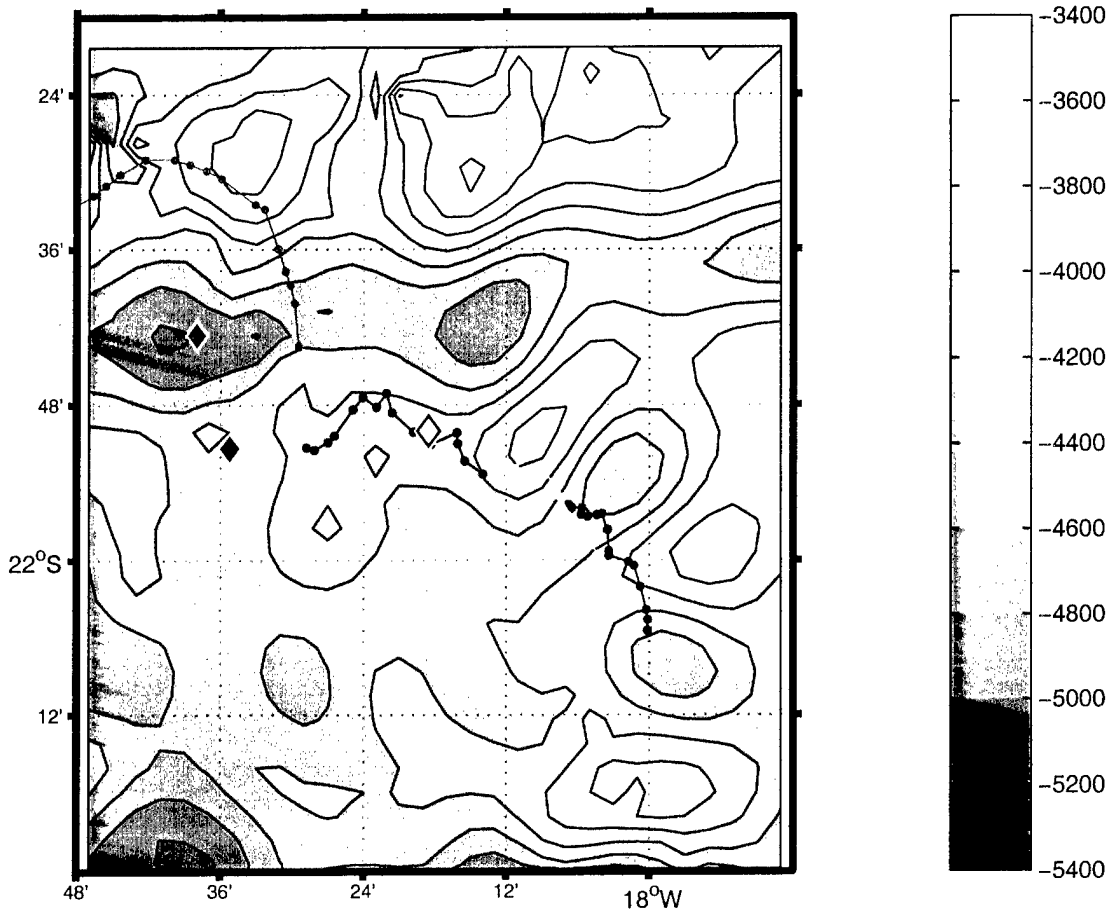

Figure 6-12. The first 16 days of each trajectory shown in Figure 6-11 are plotted using the color scheme of that Figure. Note the eastward offset from the launch position (diamonds). The depth contour intervals for the *Smith and Sandwell* (1997) bathymetry differ from those of Figure 6-11.

Table 6-1. Float speed parameters. Speed units are cm/s. *u* is eastward, *v* northward.

SN	Depth	mean *u*	mean *v*	rms *u*	rms *v*
099	3550 m	0.12	0.24	1.64	1.56
100	2800 m	1.33	-0.62	1.92	1.65
101	3130 m	1.26	-0.10	1.37	1.83

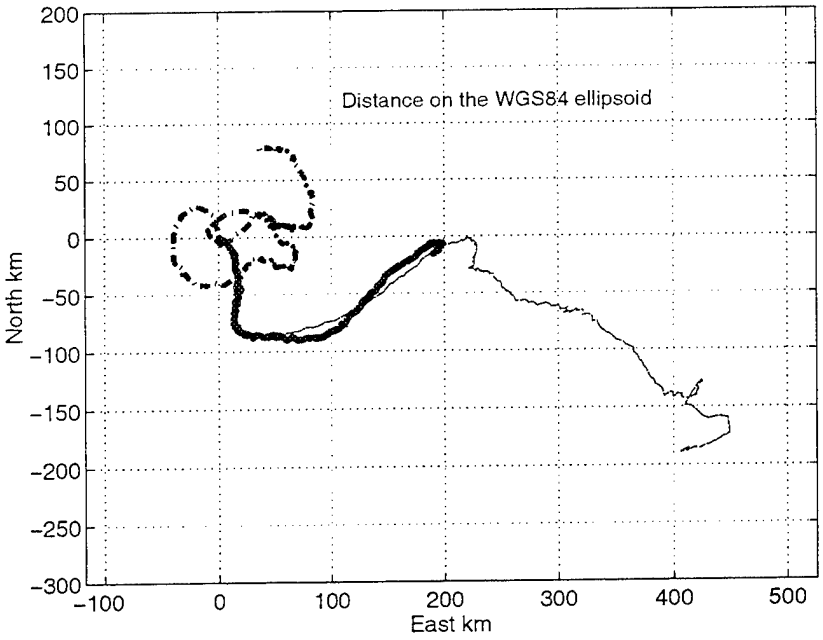

Figure 6-13. The three longest tracks are plotted in terms of distance from their origins.

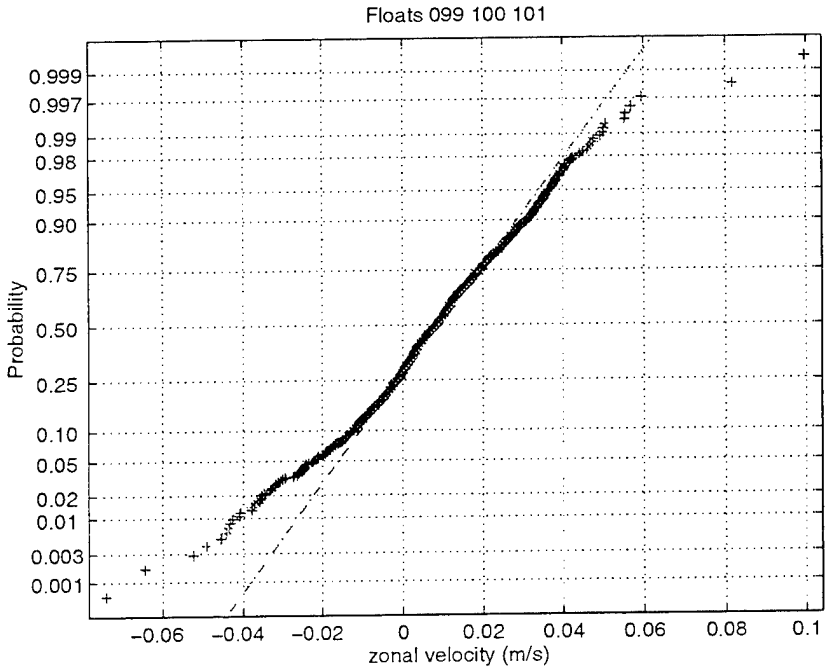

Figure 6-14. The zonal velocity probability diagram exhibits nearly normal distribution, with a slight excess of high westward values (more than 5% of the values off the line fitting a normal distribution).

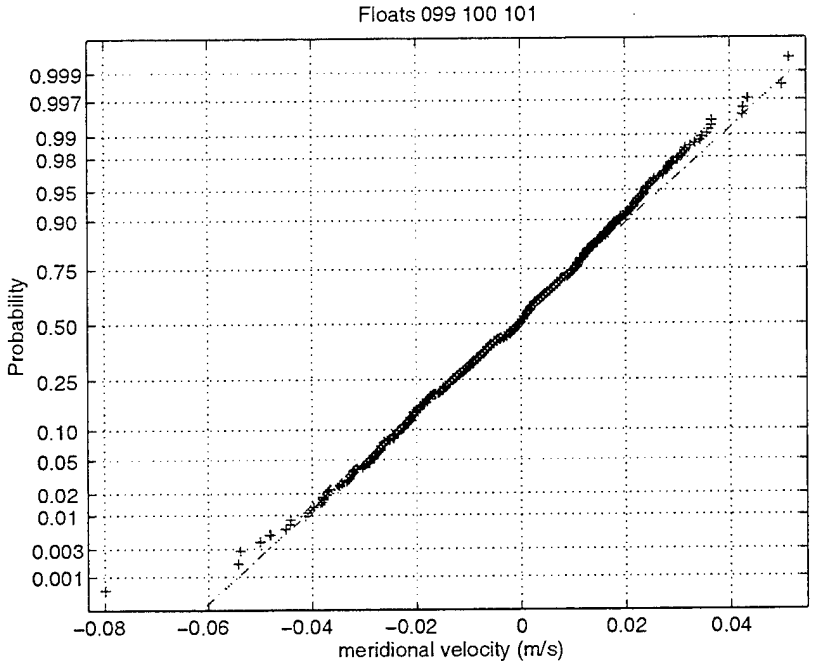

Figure 6-15. The meridional velocities are nearly normal, falling on a line in this normalized plot of the probability distribution function.

6.3. Shear and Delta-*T* Data from the Deep Floats

The rotation data can be converted to shear using algorithms derived from tow tank tests. A plot of rotation rate of a single vane being towed in a tank to the tow speed appeared in *Duda and Webb* (1997). A curve composed of two line segments passes nicely through the points, each with the form $r = ms + b$, where r is rotation rate in rev/hr, s is speed in m/s, m is the slope, and b is the r-axis intercept. The line for low speeds passes through the origin (i.e. $b = 0$). The other line connects to it at $r_k = 1.6528$. Parameters for the lines are $m_1 = 146.9$, $b_1 = 0$, $m_2 = 264.4$, and $b_2 = -1.3222$. After differencing the rotation counter, which has a least count of 1/8 revolution, over the hourly time series, the data are divided into values above and below the kink at $r = r_k$. Shear values for the BBTRE floats of length 9.5 m are then given by

$$S_n = (r - b_n)\left[\frac{2}{9.5}\right]\left[\frac{1}{m_n}\right]$$

where subscript $n = 1,2$. Figure 6-16 shows shear for the deep float SN 100. The dynamic range extends from zero to 0.0033. Figures 6-17 and 6-18 show enlargements of shorter time intervals. These sections were chosen to include a period of low shear for days 155-169 and a transition from low shear to high shear at day 159. No dominant temporal periodicity is seen.

Figure 6-19 shows the histogram of shear *(S)* and compares it to the histogram one might expect from a wavefield having a Garrett-Munk (GM) spectrum. The histogram is computed using joint normally distributed and uncorrelated shear components scaled according to GM, rather than creating a GM wavefield and then first differencing. This is sufficient for the purposes of this report. The mean GM shear for the local $N = 0.5$ cph is 5×10^{-4} s^{-1}, according to the formula of *Gregg* (1989).

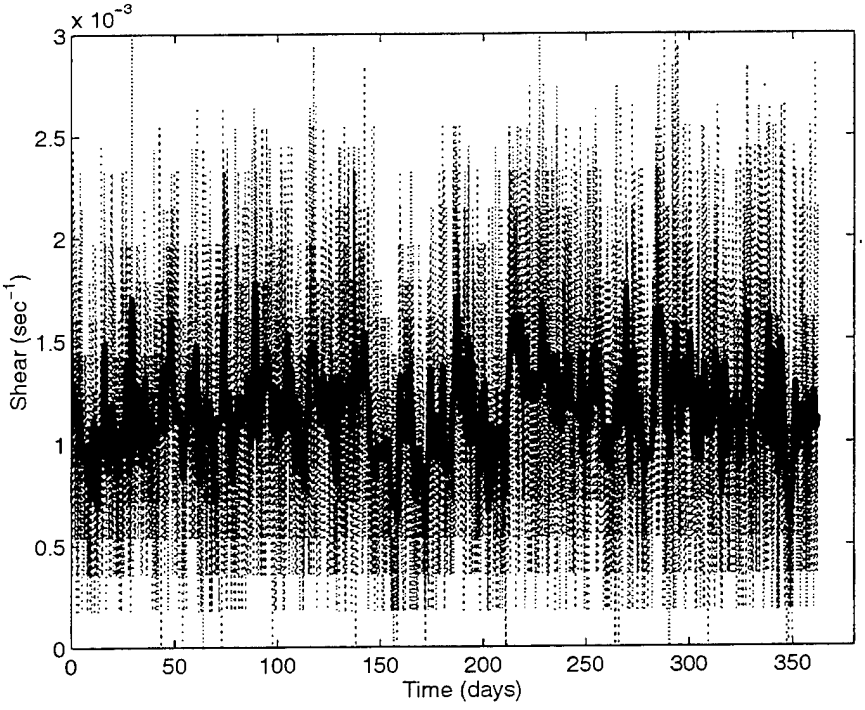

Figure 6-16. Hourly shear data from float SN 100. Unfiltered and filtered versions are shown. The filter has a one-day time scale.

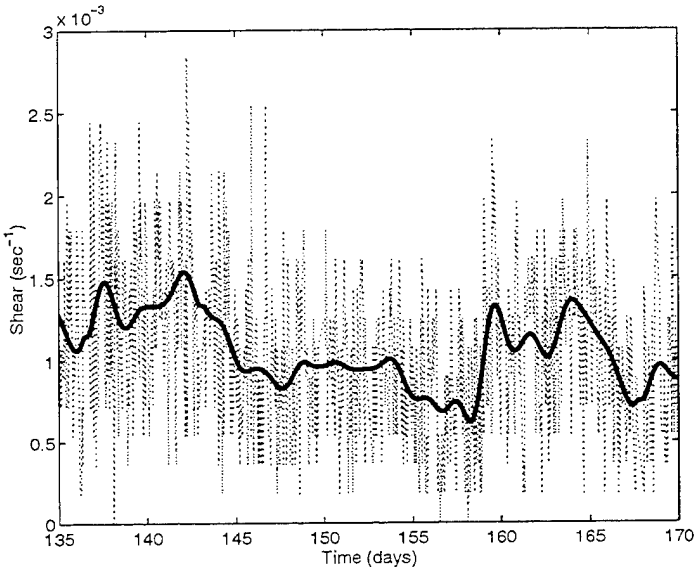

Figure 6-17. A short 35-day record of shear, filtered (one day f_c) and unfiltered.

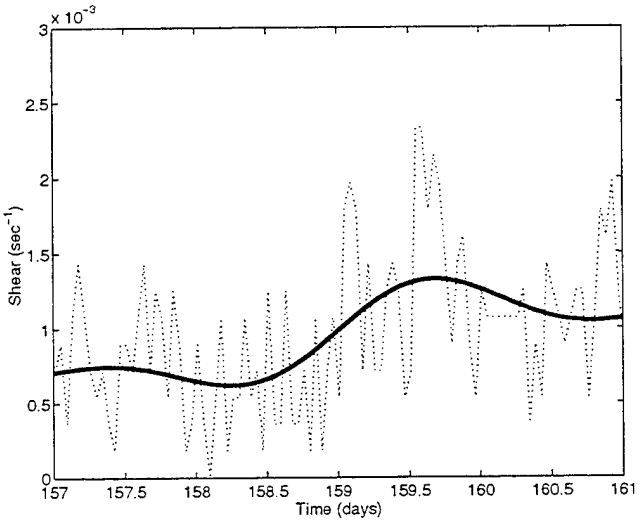

Figure 6-18. A very short section of filtered and unfiltered shear.

Figure 6-20 shows how six statistics of shear change as they are computed for various shear time series produced by different filtering. The statistics are fairly stable. The mean and standard deviation values are close to the values for the unfiltered time series which are reported in the caption. Mean shear is well constrained, but means of shear squared and shear to the fourth power are dependent on the averaging interval. This is significant because the fourth power of shear appears in the expression for wave dissipation and subsequent mixing (*Gregg* 1989, *Polzin et al.* 1995). Any filtering at all of the hourly time series significantly reduces the higher powers of shear (the second and fifth panels). Figure 6-21 shows the fourth power of the lowpass filtered shear (one-day corner period, as used in Figure 6-17), converted to internal-wave dissipation rate ε using the scaling formulas of *Gregg* (1989)

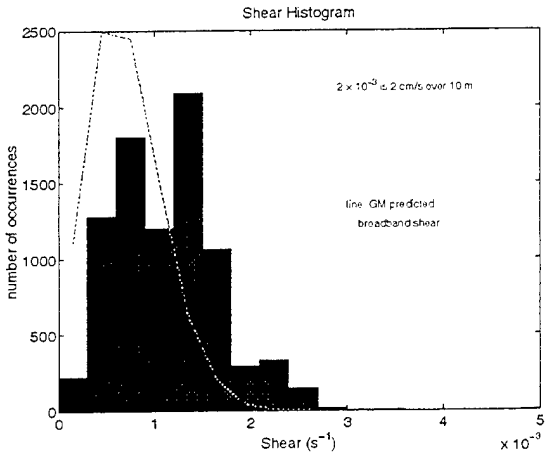

Figure 6-19. Histogram of hourly shear for float 100.

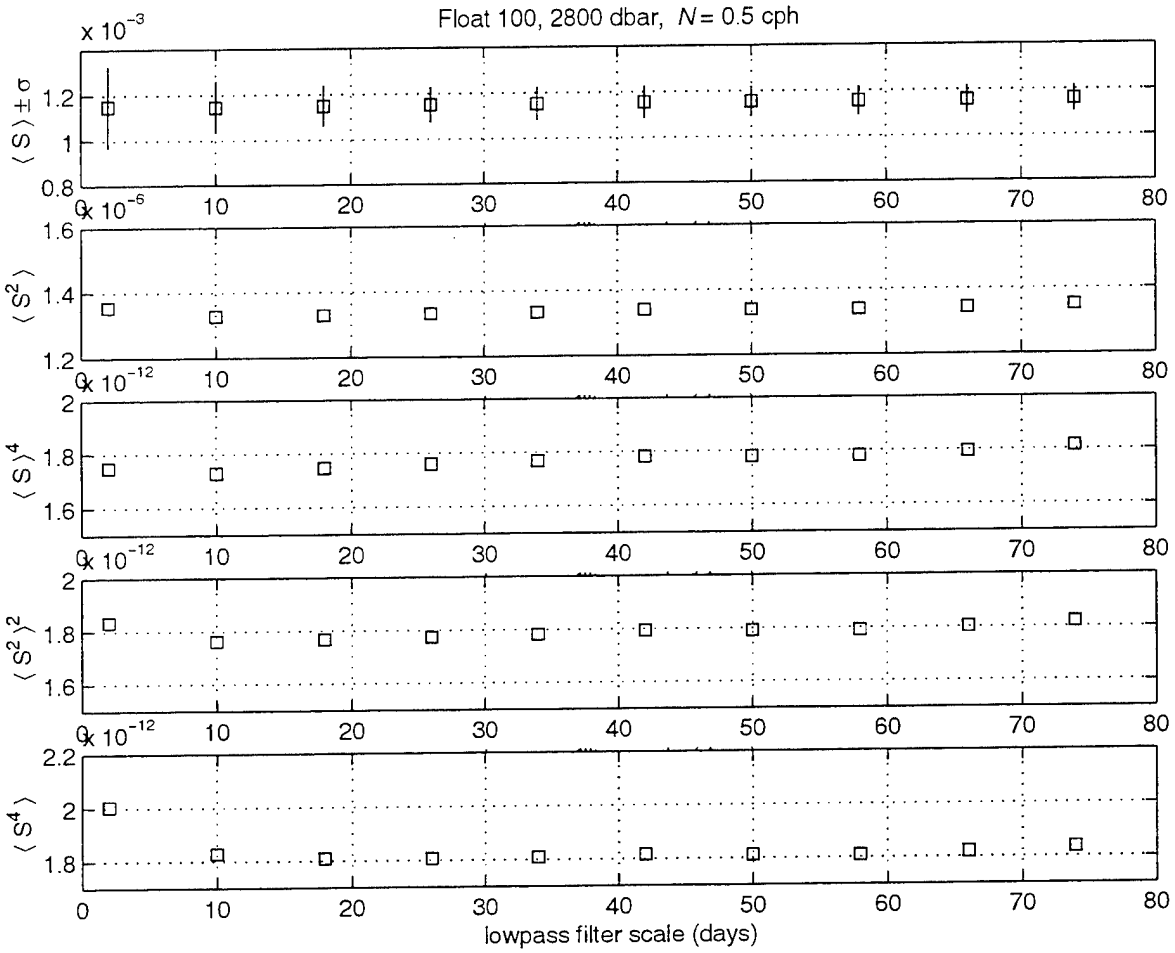

Figure 6-20. Six shear statistics for float 100 filtered time series are plotted as functions of filter time scale. The parameters computed from the *unfiltered* shear time series are (as appearing from top to bottom): mean $S = 1.15\times10^{-3}$; standard deviation 5.54×10^{-4}; mean $S^2 = 1.63\times10^{-3}$e-6; (mean $S)^4$ 1.75×10^{-12}; mean square of $S^2 = 2.65\times10^{-12}$, and mean $S^4 = 1.34\times10^{-11}$.

and/or *Polzin et al.* (1995) which are complex and not fully described here. See *Duda and Jacobs (1995)* for a discussion. The Gregg version of the dissipation rate is

$$\varepsilon_G = E_{GM}{}^2 \left(\frac{1.67}{\pi}\right) j^{*2}\, b^2 f \cosh^{-1}(N/f) N^2 \frac{\langle S^4 \rangle}{\langle S_{10\,GM}{}^4 \rangle}$$

The angle brackets denote mean computed in some manner, $E_{GM} = 6.3 \times 10^{-5}$, S_{10GM} is shear in the GM model computed at the same 10-m vertical aperture as the float shear measurement, the modal bandwidth j^* is 3, vertical scale b is 1300 m, f is the Coriolis parameter, and N is the local buoyancy frequency. This can be further converted to eddy diffusivity K using $K = \varepsilon / 5\, N^2$ (Figure 6-21). The mean of K from float 100 computed using ε_G and one-day lowpass filtered shear, raised to the fourth power, is 7.9×10^{-5} m^2/s. K can also be computed using one-day averaged S^4, where the hourly shear magnitude is exponentiated before averaging, and this is also shown in the figure. The mean of these K's is 1.7×10^{-4} m^2/s.

The power spectral density of hourly shear magnitude is shown in Figure 6-22. The curve rolls off with approximately the -½ power.

The delta-temperature measurement suffered from drift in three of the four instruments. Figures 6-23 through 6-26 show the direct output of the delta-T measurement. This has a 12-bit dynamic range (4096), with a least count of 0.5 millidegree. Three of the figures show drift that can be removed to look at high-frequency strain behavior in the water column. However, the mean delta-T can't be recovered in those cases. The mean delta-T for the other float, 101, as measured, is 84.5 millidegrees, with a standard deviation of 46 millidegrees. The sign reversals are interesting, particularly if they are real. They may only be noise, however, and the system performance should be tested. The mean ΔT value corresponds to $N = 2$ cph based on the density coefficient $d\rho / dT = -0.17$. for the *in situ* conditions. This value of N is probably not correct (too great) indicating that the calibration may be unreliable, particularly in light of the drifts seen in the other units.

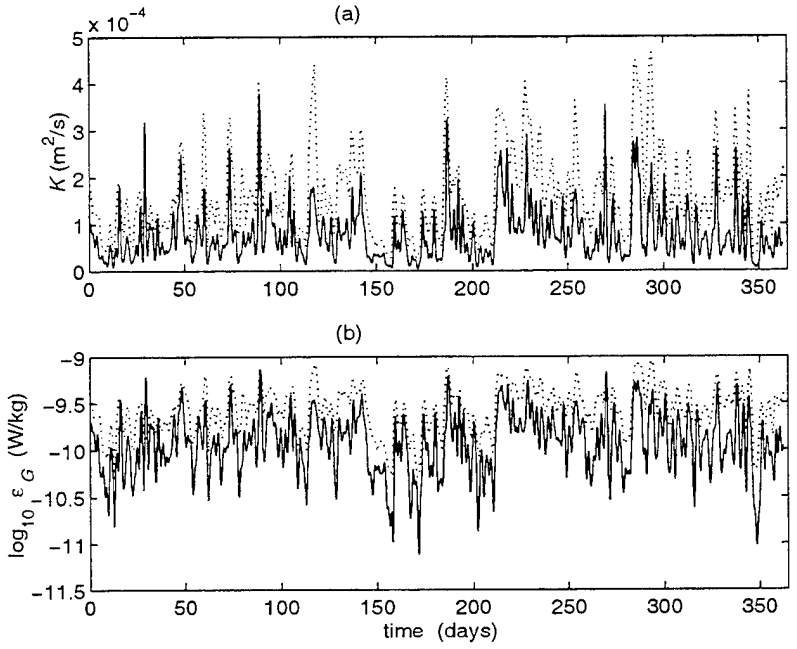

Figure 6-21. For float 100: (a) K computed from one-day lowpass filtered shear (line) and from the mean S^4 computed for each day (dotted line). (b) The same two time series are plotted using semilog format in units of dissipation rate ε_G, which is proportional to K.

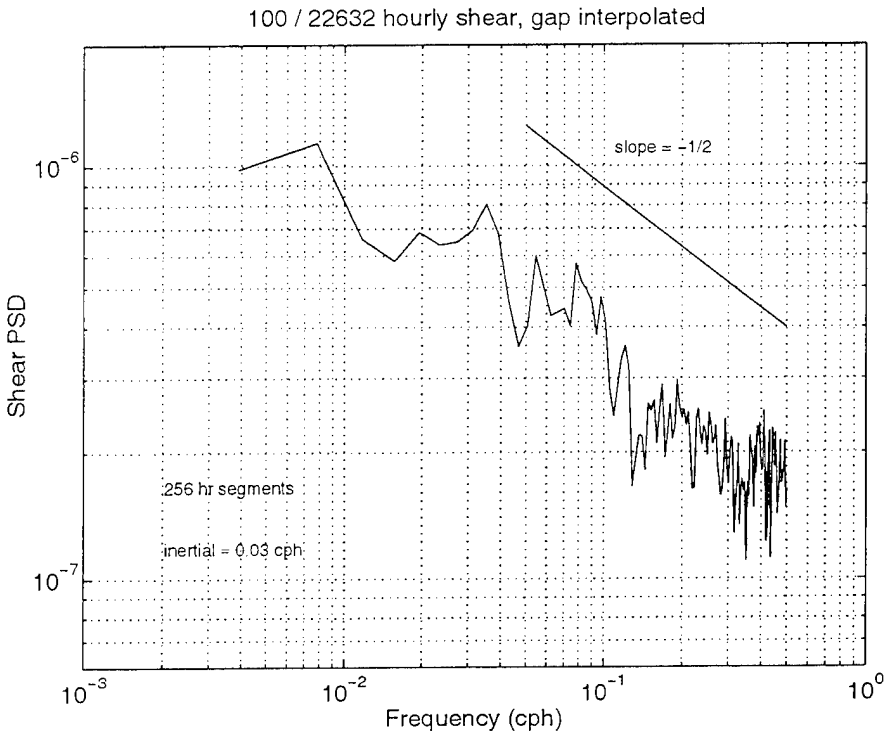

Figure 6-22. Power spectral density of shear magnitude. Power spectral density units are s^{-2}/cph.

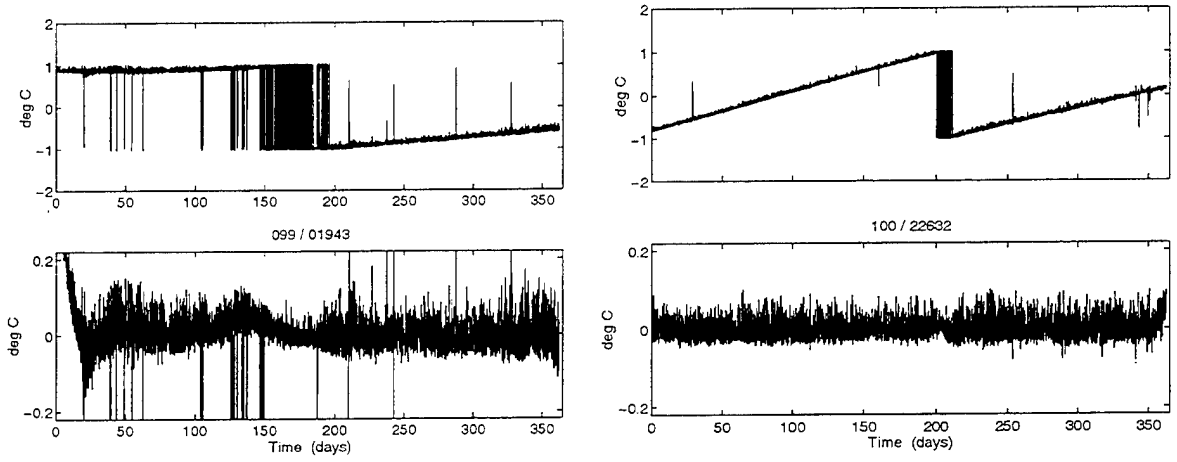

Figures 6-23 (left) and **6-24.** Untreated ΔT data (top), and filtered data (bottom), floats 099 and 100.

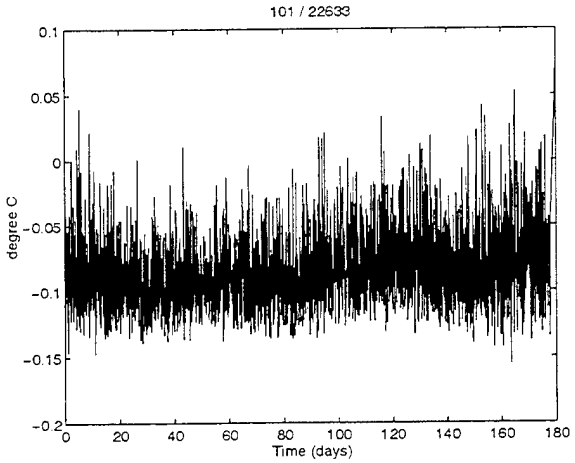

Figure 6-25 Untreated ΔT, float 101.

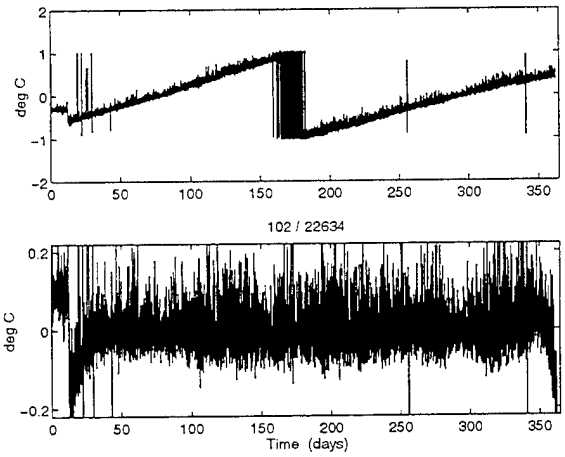

Figure 6-26. Untreated and filtered ΔT data. float 102.

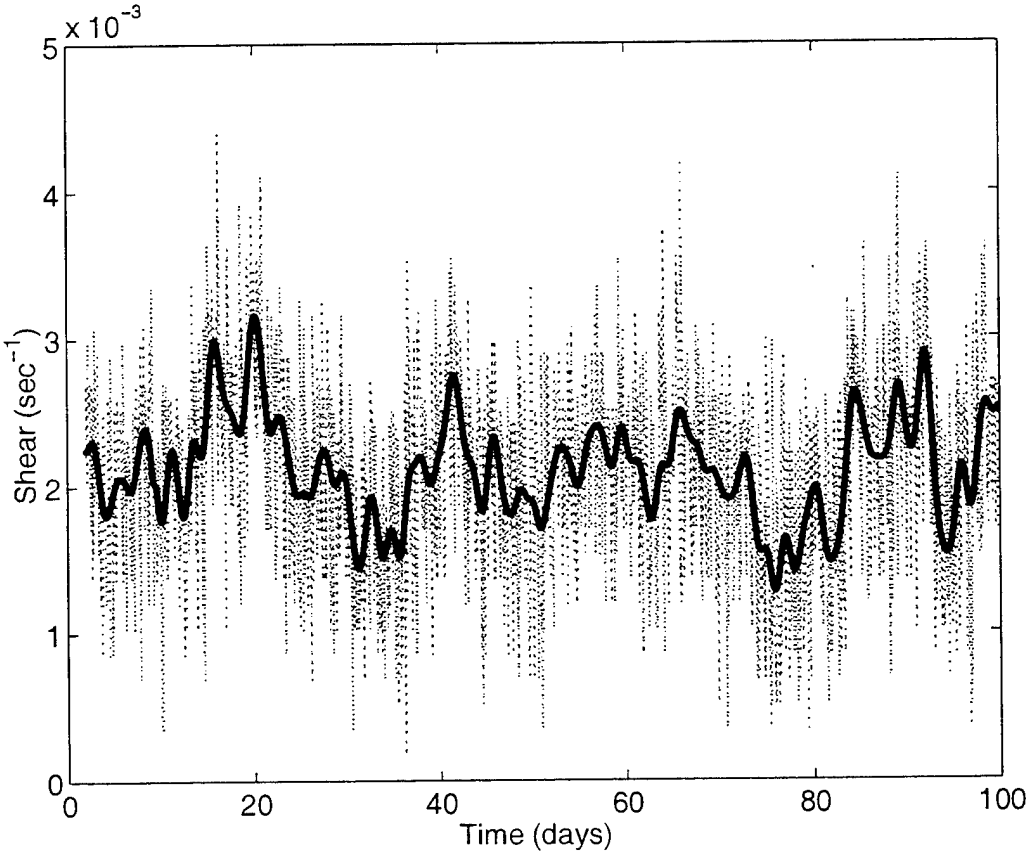

Figure 6-27. Shear record from the 1660-m depth prototype float.

6.4. Shear Data from the Shallow Float

The shear measured by the shallow float (SN 001) was highly variable, as with the deep float. Compared to that of the deep float, this shear record had a higher mean level and higher peak levels. Hourly shear from this float was never zero (below the least count level of 1/8 revolution per hour), as it was a few times at the deeper depth. Estimates of shear, computed from rotation rate using the method described in the previous subsection, are plotted in Figure 6-27. A lowpass filtered version of shear is also shown, with the lowpass filter corner period equal to one day, as used in Figure 6-17. The histogram of shear is shown in Figure 6-28. For comparison, the histogram of GM shear computed for the estimated local N of 1.14 cph is also shown.

The statistics of shear are shown in Figure 6-29. Figure 6-30 shows the spectrum of shear magnitude. As with the deep float, shear to the fourth power can be converted to internal wave dissipation rate ε_G using the Gregg formula, and further converted to K using $K = 0.2\ \varepsilon_G N^{-2}$. Time series of K and ε_G are shown in Figure 6-31. A mean K value obtained from the one-day filtered time series is 4.8×10^{-5} m^2/s. K computed from daily averages of unfiltered S^4 has a mean of 6.5×10^{-5} m^2/s. For comparison, the values obtained using GM shear are $\varepsilon_G = 5.75\times10^{-11}$ W/kg and $K = 3\times10^{-6}$ m^2/s.

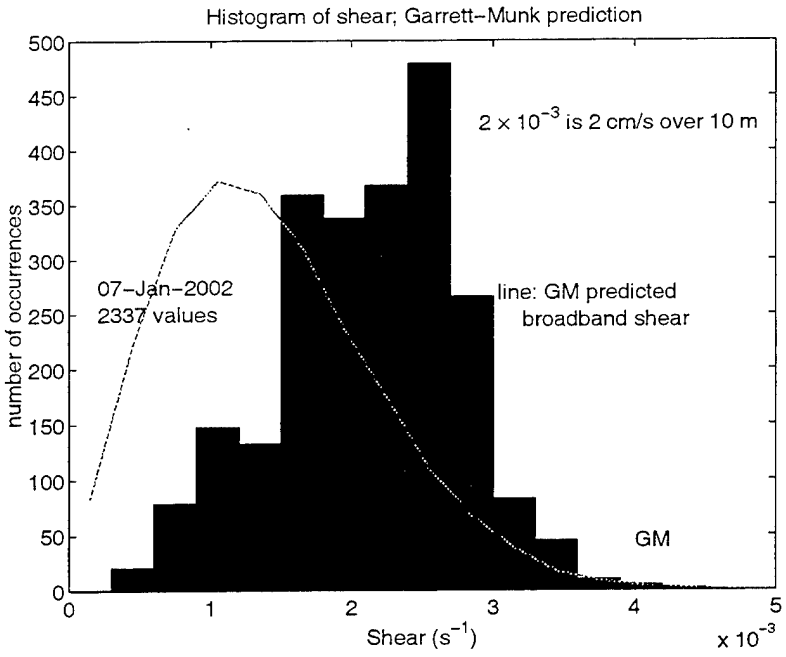

Figure 6-28. Histogram of shear from the shallow float, reference $N = 1.14$ cph.

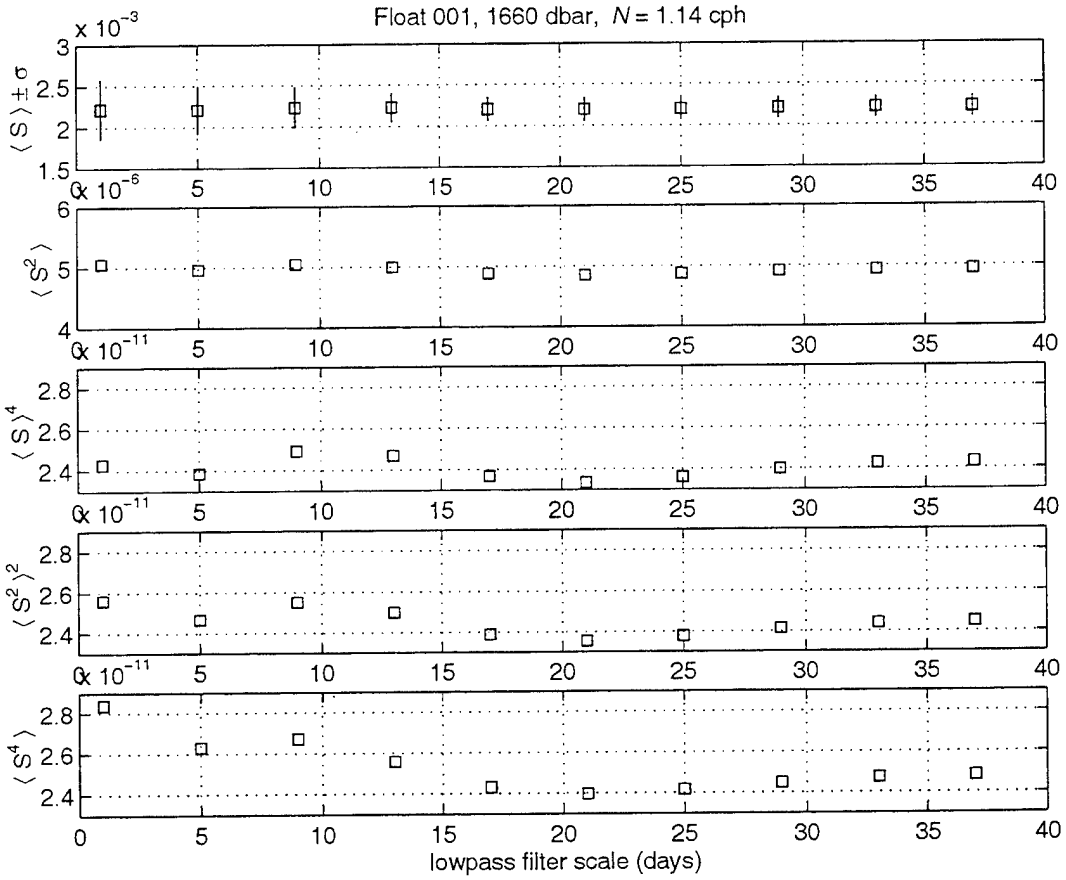

Figure 6-29. Six shear statistics for float 001 filtered time series are plotted as functions of filter time scale. The record length is 100 days. The parameters computed from the *unfiltered* shear time series are (as appearing from top to bottom): mean $S = 2.22\times10^{-3}$; standard deviation 6.78×10^{-4}; mean $S^2 = 5.39\times10^{-6}$; (mean $S)^4 = 2.43\times10^{-11}$; mean square of $S^2 = 2.90\times10^{-11}$, and mean $S^4 = 3.81\times10^{-11}$.

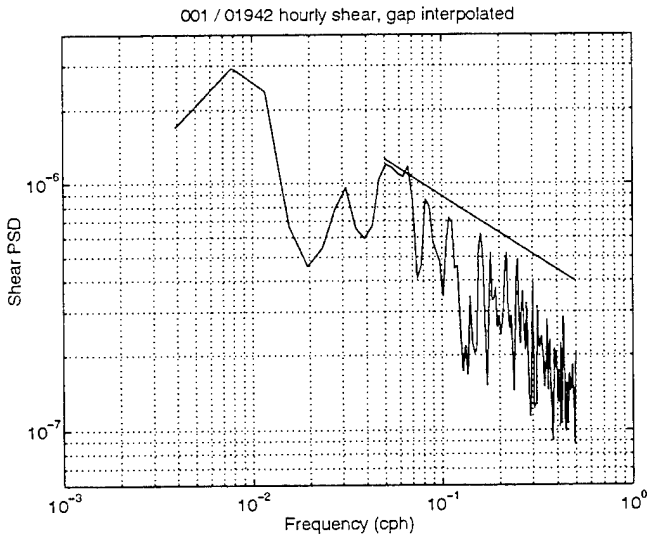

Figure 6-30. Shear spectrum from the 1660-m depth float. 256-hr segments were Fourier transformed. The reference line is identical to that in Figure 6-22.

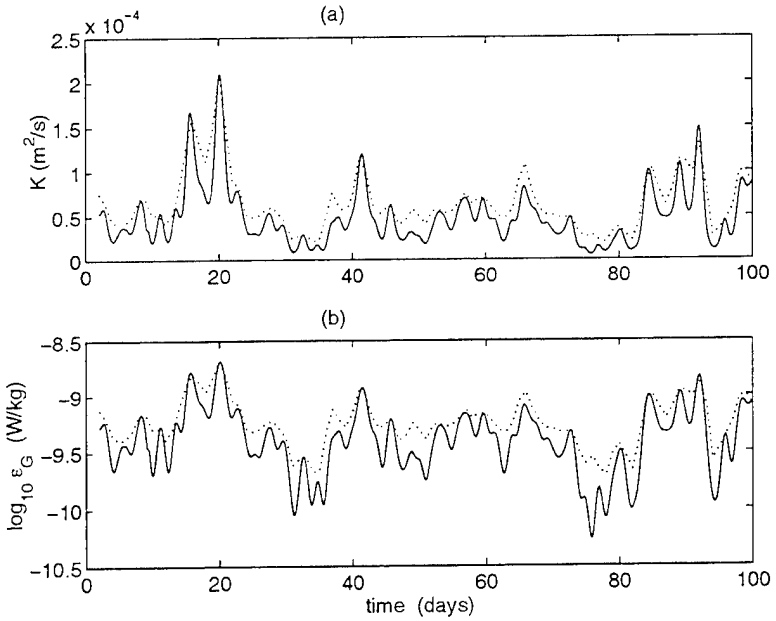

Figure 6-31. For float 001: (a) K computed from one-day lowpass filtered shear (line) and from mean S^4 computed each day (dotted line). (b) The same two time series are plotted in units of dissipation rate ε_G, which is proportional to K.

7. Ancillary Data and Interpretations

The time series of shear were collected from two floats that were moving over a seafloor of variable depth and covered many spring/neap tidal cycles. The shear records exhibit long-period temporal variability of unknown spatial or temporal origin, with red spectra. Three comparisons of shear to ancillary data will be made here. The first is between shear and float height above the bottom. The second is between shear and modeled tidal current. The third is between the shallow shear time series and atmospheric conditions.

7.1 Comparison of Shear and Height Above Bottom

In light of recent work by *St. Laurent, Toole and Schmitt* (2001), one might expect to see a tapering off of shear at increased height above the bottom and/or a correlation between the magnitude of the shear and the daily-averaged tidal current speed. Both of these comparisons are presented here for the 2800-m depth shear time series. The 1660-m depth time series will only be compared to the tidal current time series since *St. Laurent et al.* suggest a weaker vertical dependence at greater than 1000 m above the bottom. The tidal comparisons are in the next section.

St. Laurent et al. (2001) show a relation between kinetic energy dissipation rate and height above the bottom. The relation is slightly different over three classes of data: data taken above ridge crests, above fracture zone valleys, and above slopes; but a decrease of dissipation rate with height above the bottom is common to all three situations

The height above bottom (HAB) of the deep float that returned the shear record was highly variable. Figure 7-1 shows the depth of the float and the depth of the underlying seafloor, interpolated

in two dimensions from the *Smith and Sandwell* (1997) database using the float trajectory. The error in the bathymetry is of order a few hundred meters over rough areas and less over smooth areas. Figure 7-2 shows HAB together with K estimated from the float rotation (one-day lowpass filtered shear version of K). There is no immediately obvious relationship, although there is a hint of lower K between days 140 and 215, which is a period when the bathymetric deviations were less severe. The deviations remain less pronounced until day 250 but the shear and K increase, however.

To test the relationship between HAB and mixing suggested by Figure 3 of *St. Laurent et al.* (2001), means are computed for shear and K divided into six 400-m tall HAB bins. Figure 7-3 shows the result, with no detectable HAB dependence of shear or K. This is not a good direct comparison with the kinetic energy dissipation rate vs. HAB results of *St. Laurent et al.*, however, which are divided into over-slope, over-crest and over-canyon classes, which are most pronounced at HAB less than 400 m, which is entirely within our first bin, and which are weak for HAB greater than 1000 m.

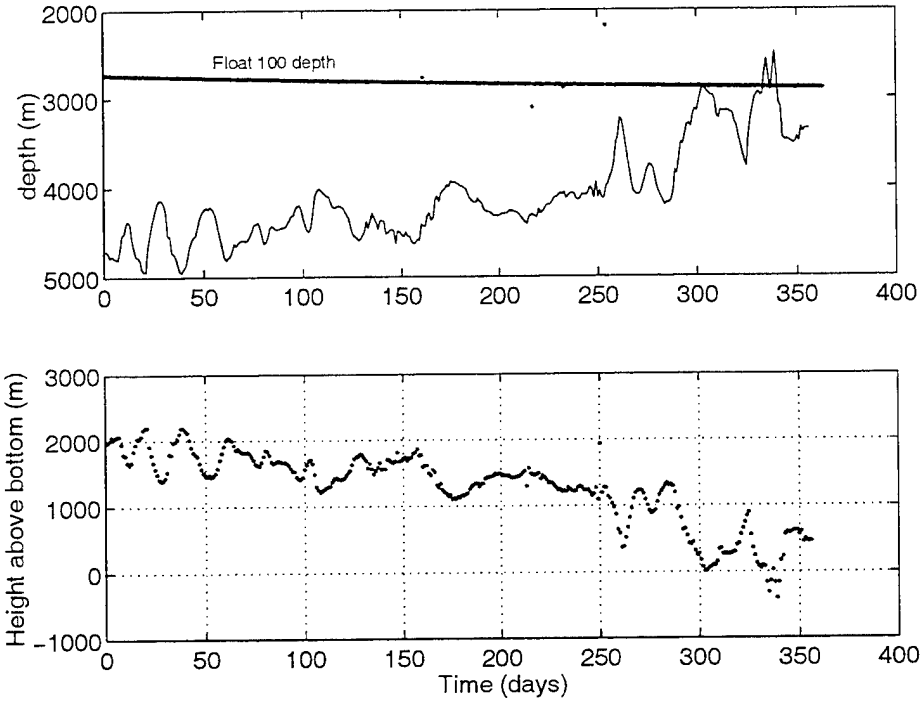

Figure 7-1. (Top) Float 100 depth and seafloor depth beneath the float as functions of time. (Bottom) Float height above the bottom.

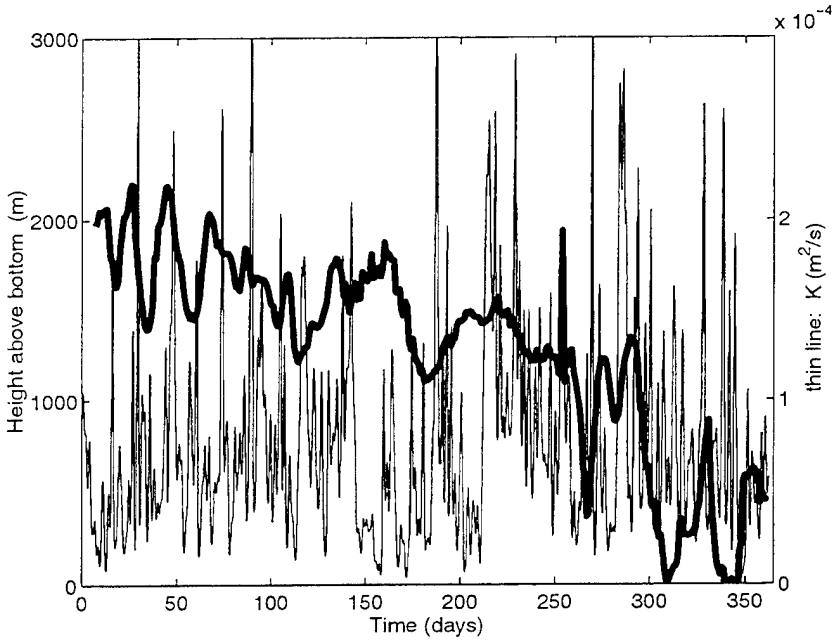

Figure 7-2. *K* values from Figure 6-21 (thin line, right axis) are compared with height above bottom (thick line, left axis).

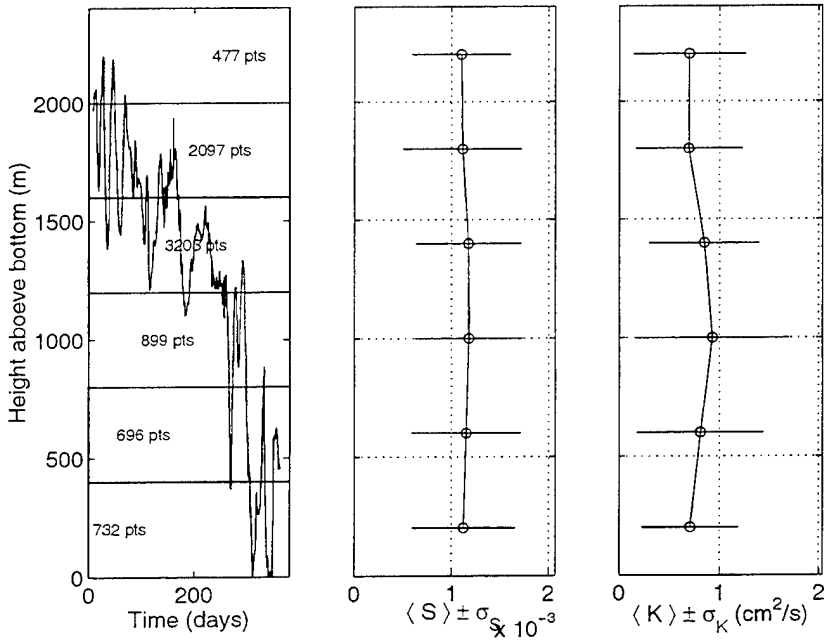

Figure 7-3. (Left) The HAB of float 100 is plotted as a function of time. The numbers of shear values collected in each of six 400-m tall bins are listed. (Middle) Mean lowpass filtered shear ± standard deviation for the six depth bins. (Right) Means over the same bins of *K* values computed as in Figure 6.21.

7.2 Comparison of Shear and Tidal Current

St. Laurent et al. (2001) also show a correlation between predicted daily averaged tidal current speeds and depth integrated dissipation rate, so the next comparison is between temporally varying tidal currents and shear. Figure 7-4 shows at the top the fourth power of one-day filtered shear from the shallow float (SN 001), which is proportional to ε_G and K. At the bottom the square of lowpass filtered tidal current speed is shown. The tidal current speed is computed beginning with eight constituent amplitudes and phases from the *TPXO.3* model of *Egbert, Bennett and Foreman* (1994). The program *Tidhar* is used to generate the time series. A partial listing of *Tidhar* output is given in the Appendix. Eastward and northward *TPXO* velocity amplitudes and phases at the BBTRE site from eight tidal constituents are fed into the equilibrium tidal code, which estimates additional constituent amplitudes and phases. Time series of each velocity component are computed from the complete set of constituents. The spring/neap tidal current variability is evident in Figure 7-4. The square is plotted because it is proportional to bottom drag force under the assumption of a quadratic drag law, which is in turn presumed to be proportional to the energy flux of a radiated wavefield (*Bell,* 1974). The two time series do not resemble one another, but they do have the same dynamic ranges of fluctuation.

Figure 7-5 shows the shear/tide comparison for the deep float (SN 100) and is a direct analogue of Figure 7-4. As with the shallow float data, the relative magnitudes of the fluctuations for the two series (current speed squared and the fourth power of shear) are similar. The first portion of the Figure 7-5 data are plotted in normalized form in Figure 7-6. The asterisks mark the peaks in tidal current. Following each peak is a spike of S^4, occurring three to eight days after the tidal peak, suggesting a link between the two.

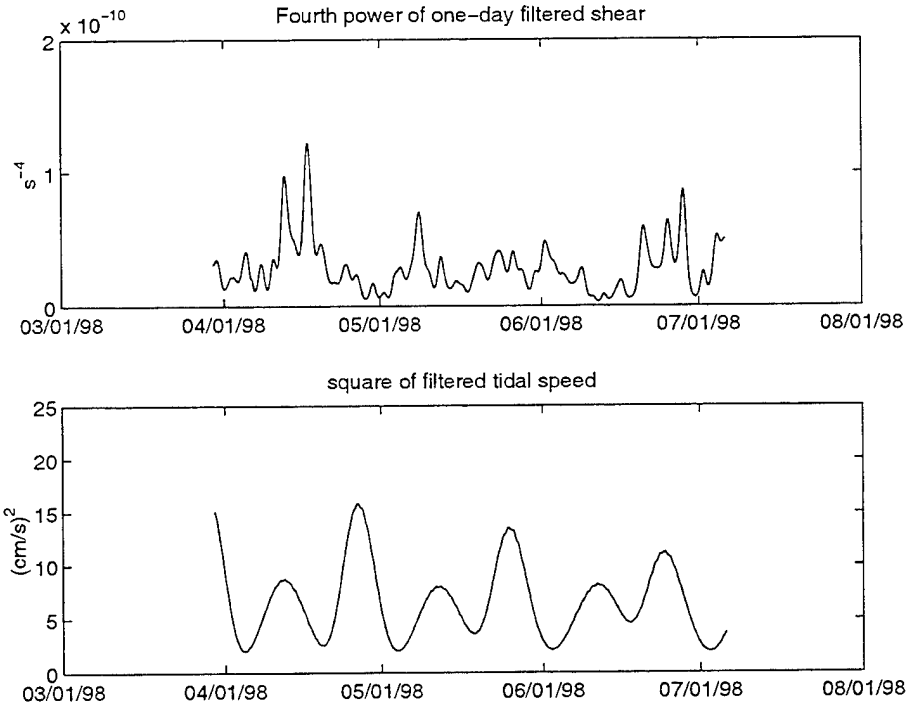

Figure 7-4. (Top) S^4 from the shallow float. (Bottom) Filtered tidal current speed squared.

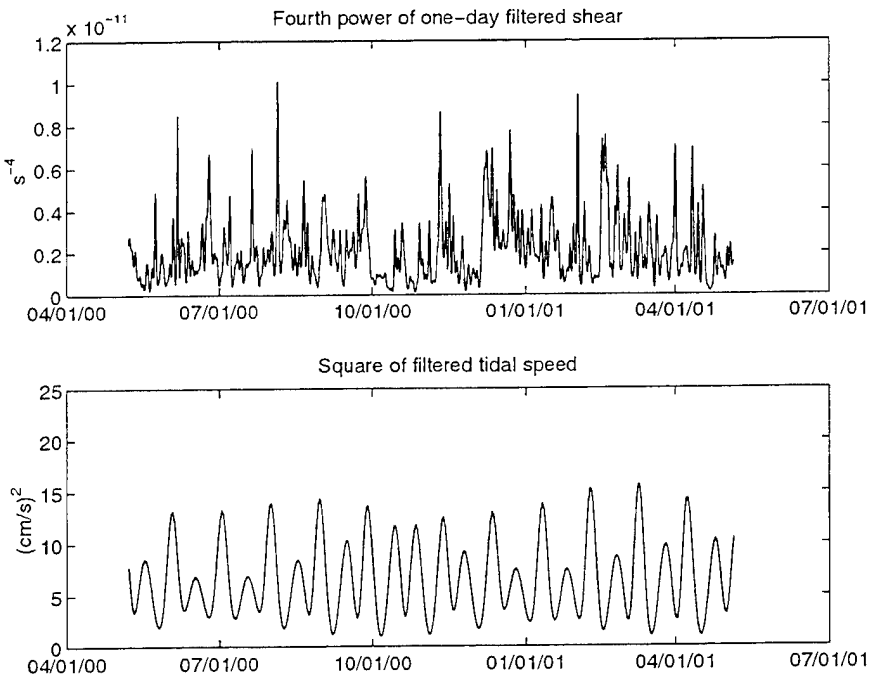

Figure 7-5. (Top) S^4 from deep float 100. (Bottom) Filtered tidal current speed squared.

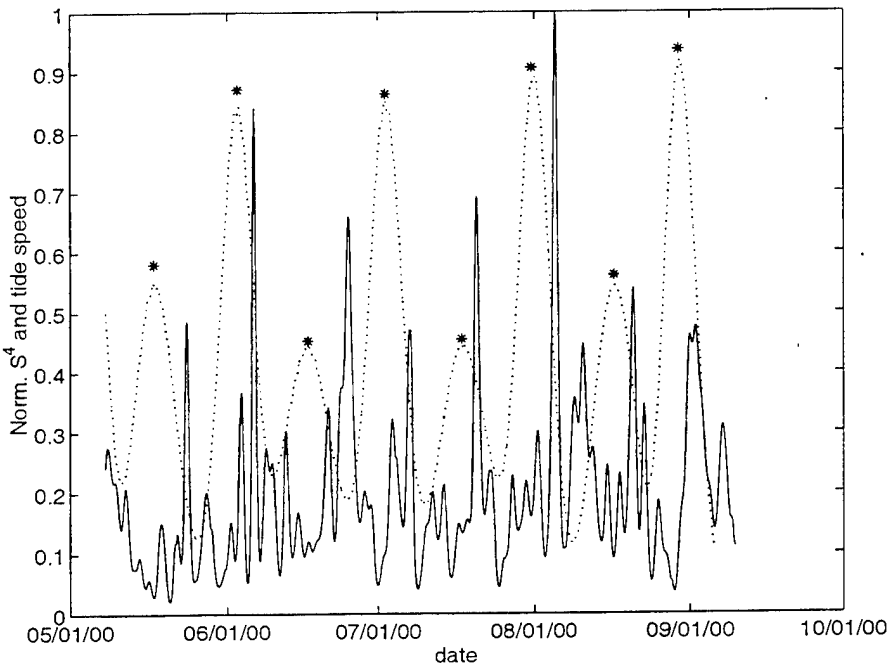

Figure 7-6. S^4 and normalized tidal speed from the previous figure are shown. Only the first four months' data are plotted.

7.3. Comparison of 1660-m Shear and Atmospheric Conditions

The shear from the shallow float displayed five strong peaks, with the two strongest peaks occurring in March (Figure 7-4). This is autumn at the float location. To investigate whether the passage of storms might have generated pulses of internal waves, the time series can be compared with atmospheric condition databases. The data used here are the NCEP/NCAR CDAS-1 (National Centers for Environmental Prediction/National Center for Atmospheric Research Climate Data Assimilation System) daily reanalysis data for BBTRE locations 20° S, 17.5° W and 20° S, 17° W. These were downloaded from the web. Not all data types are available at all locations, thus the two locations.

Data that were downloaded were (1) Intrinsic mean sea level pressure, (2) 1000-mb meridional and zonal winds, and (3) 10-m above ground meridional and zonal winds. Figure 7-7 shows the atmospheric pressure estimated for the area. The fourth power of filtered shear time series is also reproduced (proportional to K). Two low-pressure events pass over the area in March. The second of the two high S^4 (or K) peaks follows the first event, but the first peak precedes that event and no S^4 peak follows the second low-pressure event.

The wind speed and wind stress bear less similarity to the S^4 time series than the pressure. The reanalyzed wind speed time series for 1000 mbar is plotted with S^4 in Figure 7-8. The two records are poorly correlated overall, and the peaks in wind speed are not accompanied by shear peaks. Figure 7-9 shows the wind stress computed from the 10-m reanalysis wind speed using the TOGA-COARE algorithm (*Fairall et al.*, 1996). The peaks in stress and in S^4 do not align. The only indication of atmospheric forcing of internal-wave shear from these data-assimilated model products is in the pressure record, which shows low pressure near the time of one of the S^4 peaks.

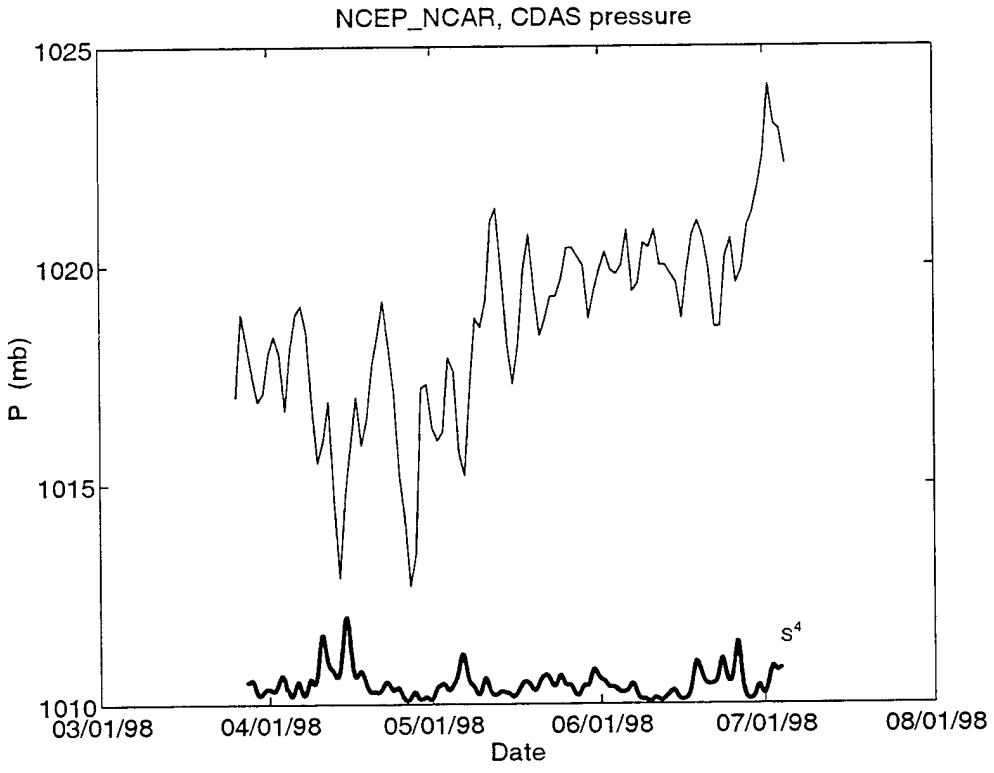

Figure 7-7. Time series of reanalysis barometric pressure at the site of float 001 is plotted. The fourth power of one-day filtered shear is reproduced at the bottom with arbitrary scaling.

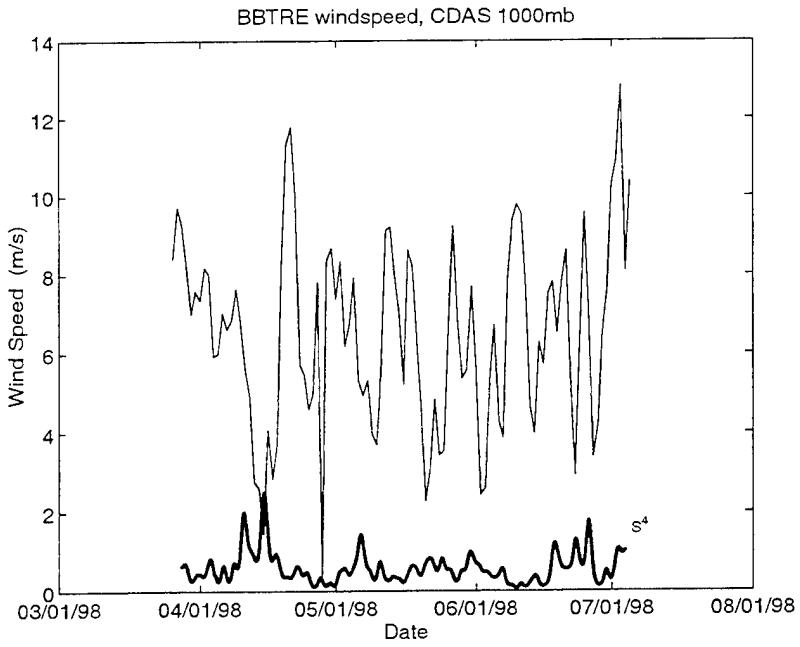

Figure 7-8. The time series of reanalyzed wind speed at 1000 mb is shown. The fourth power of filtered shear is also shown with an arbitrary scale.

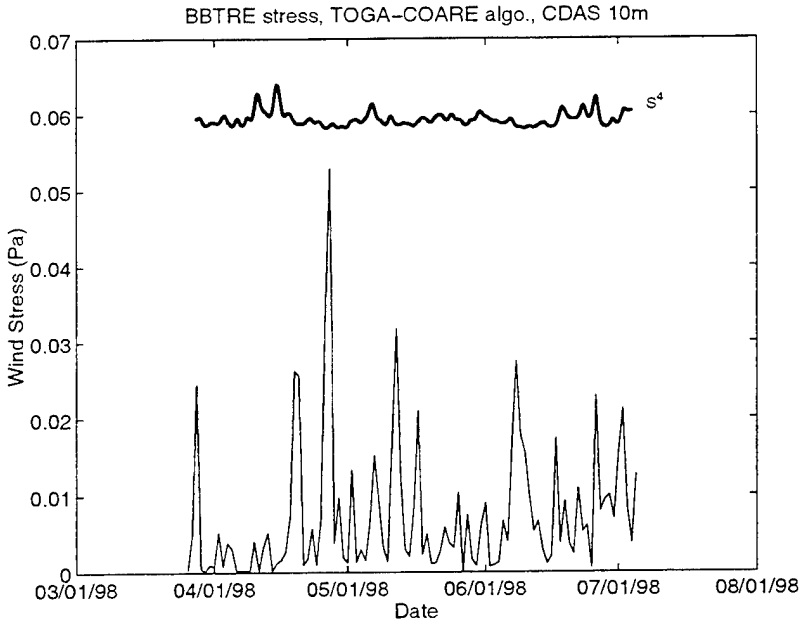

Figure 7-9. The time series of wind stress is shown, computed from 10-m height reanalysis wind speed using the TOGA-COARE algorithm. The fourth power of shear is reproduced as in the previous figure.

Appendix: *Tidhar* Output

A partial listing of *Tidhar* output is reproduced below. Eight tidal constituent parameters for east and north velocities (u and v) at 20° S, 17° W from *TPXO.3* are printed out after being input. These are annotated below. Additional constituents are predicted by the program for one-year intervals and the lengthened lists of constituent parameters are then output. The constituents are predicted to change over time due to astronomical conditions. Hourly time series of u and v for the period 1 January 1996 to 11 January 2002 were output to separate data files. Dr. James D. Irish provided this *Tidhar* output listing and the tidal velocity time series.

```
Tidhar:  01/11/**   15:18
last update:  22 Feb 1997

start time
    jan  1, 1996    0.00 hours          841512.00 julian hours
end time
    jan 11, 2002    0.00 hours          894360.00 julian hours

following constituents supplied by user

  constituent     h       g (deg)
    M2        25.716     -37.78
    S2         9.502     -20.02
    N2         5.380     -42.96
    K2         2.540     -26.31
    K1         1.390     -96.90
    O1         1.000    -175.06
    P1         0.417    -103.60
    Q1         0.210     137.71
```

Eastward (u) parameters from *TPXO.3*

***h* units mm/s**

```
section   1   start time= 841512.00   end time= 850277.00
 prediction based on following constituents

symbol     freq(cpd)    coeff      h       g(deg)     ampl   in.phase  freq(rad/dt)
 2Q1      0.85695241   0.0097    0.026  -175.06     0.021      38.87    0.22434962
 SIGMA1   0.86180932   0.0061    0.016  -175.06     0.013      37.67    0.22562115
 Q1       0.89324406   0.0730    0.210   137.71     0.170     206.58    0.23385075
 RO1      0.89810097   0.0142    0.038  -175.06     0.031     158.15    0.23512228
 O1       0.92953571   0.3771    1.000  -175.06     0.812     279.84    0.24335188
 M1       0.96644626   0.0317    0.084  -175.06     0.061      88.13    0.25301504
 PI1      0.99452431   0.0103    0.027   -96.90     0.027      89.90    0.26036586
 P1       0.99726209   0.1755    0.417  -103.60     0.417      93.67    0.26108261
 K1       1.00273791   0.5305    1.390   -96.90     1.231     109.15    0.26251617
 J1       1.03902955   0.0297    0.078   -96.90     0.065     230.92    0.27201730
 OO1      1.07594011   0.0163    0.043   -96.90     0.021     199.20    0.28168046
 2N2      1.85969032   0.0235    0.719   -42.96     0.745     280.30    0.48686579
 MU2      1.86454723   0.0219    0.670   -42.96     0.694     279.10    0.48813732
 N2       1.89598197   0.1759    5.380   -42.96     5.578      40.79    0.49636692
 NU2      1.90083887   0.0341    0.965   -37.78     1.001      34.40    0.49763845
 M2       1.93227361   0.9085   25.716   -37.78    26.665     156.09    0.50586805
 L2       1.96856526   0.0251    0.710   -37.78     0.787     104.51    0.51536918
 T2       1.99726222   0.0248    0.557   -20.02     0.557      22.97    0.52288203
 S2       2.00000000   0.4227    9.502   -20.02     9.502      20.04    0.52359877
 K2       2.00547582   0.1151    2.540   -26.31     1.910     230.37    0.52503234
```

section 2 start time= 850278.00 end time= 859043.00
prediction based on following constituents

symbol	freq(cpd)	coeff	h	g(deg)	ampl	in.phase	freq(rad/dt)
2Q1	0.85695241	0.0097	0.026	-175.06	0.021	44.31	0.22434962
SIGMA1	0.86180932	0.0061	0.016	-175.06	0.013	321.74	0.22562115
Q1	0.89324406	0.0730	0.210	137.71	0.169	304.01	0.23385075
RO1	0.89810097	0.0142	0.038	-175.06	0.030	174.21	0.23512228
O1	0.92953571	0.3771	1.000	-175.06	0.807	109.25	0.24335188
M1	0.96644626	0.0317	0.084	-175.06	0.083	70.65	0.25301504
PI1	0.99452431	0.0103	0.027	-96.90	0.027	179.90	0.26036586
P1	0.99726209	0.1755	0.417	-103.60	0.417	183.66	0.26108261
K1	1.00273791	0.5305	1.390	-96.90	1.227	195.66	0.26251617
J1	1.03902955	0.0297	0.078	-96.90	0.064	47.46	0.27201730
OO1	1.07594011	0.0163	0.043	-96.90	0.021	178.90	0.28168046
2N2	1.85969032	0.0235	0.719	-42.96	0.746	10.29	0.48686579
MU2	1.86454723	0.0219	0.670	-42.96	0.695	287.72	0.48813732
N2	1.89598197	0.1759	5.380	-42.96	5.582	222.76	0.49636692
NU2	1.90083887	0.0341	0.965	-37.78	1.002	135.01	0.49763845
M2	1.93227361	0.9085	25.716	-37.78	26.683	70.05	0.50586805
L2	1.96856526	0.0251	0.710	-37.78	0.654	109.09	0.51536918
T2	1.99726222	0.0248	0.557	-20.02	0.557	202.98	0.52288203
S2	2.00000000	0.4227	9.502	-20.02	9.502	200.04	0.52359877
K2	2.00547582	0.1151	2.540	-26.31	1.899	44.08	0.52503234

... sections 3-7 deleted

filename	BBTREU.PRD
date	01/11/**
time	15:18:44
start	841512.00000
finish	894360.00000
num	52849
inc	1.00000E+00

---

start time
jan 1, 1996 0.00 hours 841512.00 julian hours
end time
jan 11, 2002 0.00 hours 894360.00 julian hours

following constituents supplied by user

constituent	h	g (deg)
M2	21.347	81.05
S2	7.567	99.55
N2	4.906	69.74
K2	1.983	95.53
K1	1.629	167.63
O1	3.128	134.35
P1	0.590	161.53
Q1	0.794	110.33

Northward (v) parameters from *TPXO.3*

***h* units mm/s**

section 1 start time= 841512.00 end time= 850277.00
prediction based on following constituents

symbol	freq(cpd)	coeff	h	g(deg)	ampl	in.phase	freq(rad/dt)
2Q1	0.85695241	0.0097	0.080	134.35	0.065	89.46	0.22434962
SIGMA1	0.86180932	0.0061	0.051	134.35	0.041	88.25	0.22562115
Q1	0.89324406	0.0730	0.794	110.33	0.645	233.96	0.23385075
RO1	0.89810097	0.0142	0.118	134.35	0.096	208.74	0.23512228
O1	0.92953571	0.3771	3.128	134.35	2.541	330.42	0.24335188
M1	0.96644626	0.0317	0.263	134.35	0.191	138.72	0.25301504
PI1	0.99452431	0.0103	0.032	167.63	0.032	185.37	0.26036586
P1	0.99726209	0.1755	0.590	161.53	0.590	188.53	0.26108261
K1	1.00273791	0.5305	1.629	167.63	1.442	204.63	0.26251617
J1	1.03902955	0.0297	0.091	167.63	0.076	326.39	0.27201730
OO1	1.07594011	0.0163	0.050	167.63	0.025	294.67	0.28168046
2N2	1.85969032	0.0235	0.656	69.74	0.680	167.60	0.48686579
MU2	1.86454723	0.0219	0.611	69.74	0.633	166.40	0.48813732
N2	1.89598197	0.1759	4.906	69.74	5.088	288.09	0.49636692
NU2	1.90083887	0.0341	0.801	81.05	0.831	275.57	0.49763845
M2	1.93227361	0.9085	21.347	81.05	22.134	37.26	0.50586805
L2	1.96856526	0.0251	0.590	81.05	0.653	345.68	0.51536918
T2	1.99726222	0.0248	0.444	99.55	0.444	263.40	0.52288203
S2	2.00000000	0.4227	7.567	99.55	7.567	260.47	0.52359877
K2	2.00547582	0.1151	1.983	95.53	1.491	108.54	0.52503234

section 2 start time= 850278.00 end time= 859043.00
prediction based on following constituents

symbol	freq(cpd)	coeff	h	g(deg)	ampl	in.phase	freq(rad/dt)
2Q1	0.85695241	0.0097	0.080	134.35	0.065	94.89	0.22434962
SIGMA1	0.86180932	0.0061	0.051	134.35	0.041	12.32	0.22562115
Q1	0.89324406	0.0730	0.794	110.33	0.641	331.38	0.23385075
RO1	0.89810097	0.0142	0.118	134.35	0.095	224.79	0.23512228
O1	0.92953571	0.3771	3.128	134.35	2.526	159.83	0.24335188
M1	0.96644626	0.0317	0.263	134.35	0.261	121.24	0.25301504
PI1	0.99452431	0.0103	0.032	167.63	0.032	275.37	0.26036586
P1	0.99726209	0.1755	0.590	161.53	0.590	278.53	0.26108261
K1	1.00273791	0.5305	1.629	167.63	1.438	291.14	0.26251617
J1	1.03902955	0.0297	0.091	167.63	0.076	142.94	0.27201730
OO1	1.07594011	0.0163	0.050	167.63	0.024	274.37	0.28168046
2N2	1.85969032	0.0235	0.656	69.74	0.680	257.59	0.48686579
MU2	1.86454723	0.0219	0.611	69.74	0.634	175.03	0.48813732
N2	1.89598197	0.1759	4.906	69.74	5.091	110.06	0.49636692
NU2	1.90083887	0.0341	0.801	81.05	0.831	16.19	0.49763845
M2	1.93227361	0.9085	21.347	81.05	22.149	311.23	0.50586805
L2	1.96856526	0.0251	0.590	81.05	0.542	350.26	0.51536918
T2	1.99726222	0.0248	0.444	99.55	0.444	83.41	0.52288203
S2	2.00000000	0.4227	7.567	99.55	7.567	80.47	0.52359877
K2	2.00547582	0.1151	1.983	95.53	1.483	282.24	0.52503234

... sections 3-7 deleted

filename	BBTREV.PRD
date	01/11/**
time	15:18:45
start	841512.00000
finish	894360.00000
num	52849
inc	1.00000E+00

References

Bell, T. H., Lee waves in stratified flows with simple harmonic time dependence, *J. Fluid Mech.*, **67**, 705-722, 1975.

Bracco, A., J. H. LaCasce and A. Provenzale, Velocity probability density functions for oceanic floats, *J. Phys. Oceanogr.*, **30**, 461-474, 1975.

Duda, T. F., and D. C. Jacobs, Comparison of shear measurements and mixing predictions with a direct observation of diapycnal mixing in the Atlantic thermocline, *J. Geophys. Res.*, **100,** 13,481-13-498, 1995.

Duda, T. F, and D. C. Webb, The drifting, rotating deep-ocean shearmeter, in *Oceans '97 Conference Proceedings,* IEEE/MTS, 796-801, 1997.

Egbert, G. D., A. F. Bennett, and M. G. G. Foreman, TOPEX/POSEIDON tides estimated using a global inverse model, *J. Geophys. Res.*, **99,** 24,821-24,852, 1994.

Fairall, C. W., E. F. Bradley, D.P. Rogers, J. B. Edson, and G. S. Young, Bulk parameterization of air-sea fluxes for TOGA COARE, *J. Geophys. Res.*, **101**, 3747-3764, 1996.

Goodman, L., and E. R. Levine, Vertical motion of neutrally buoyant floats, *J. Atmos. Oceanic Technol.*, **7**, 38-49, 1990.

Gregg, M. C., Scaling turbulent dissipation in the thermocline, *J. Geophys. Res.*, **94**, 9686-9698, 1989.

Polzin, K. L., J. M. Toole and R. W. Schmitt, Finescale parameterizations of turbulent dissipation, *J. Phys. Oceanogr.*, **25**, 306-328, 1995.

St. Laurent, L. C., J. M. Toole, and R. W. Schmitt, Buoyancy forcing by turbulence above rough topography in the abyssal Brazil Basin, *J. Phys. Oceanogr.*, **31**, 3476-3495, 2001.

Smith, W. H. F., and D. T. Sandwell, Global seafloor topography from satellite altimetry and ship depth soundings, *Science,* **277**, 1956-1962, 1997.

DOCUMENT LIBRARY

Distribution List for Technical Report Exchange – July 1998

University of California, San Diego
SIO Library 0175C
9500 Gilman Drive
La Jolla, CA 92093-0175

Hancock Library of Biology & Oceanography
Alan Hancock Laboratory
University of Southern California
University Park
Los Angeles, CA 90089-0371

Gifts & Exchanges
Library
Bedford Institute of Oceanography
P.O. Box 1006
Dartmouth, NS, B2Y 4A2, CANADA

NOAA/EDIS Miami Library Center
4301 Rickenbacker Causeway
Miami, FL 33149

Research Library
U.S. Army Corps of Engineers
Waterways Experiment Station
3909 Halls Ferry Road
Vicksburg, MS 39180-6199

Marine Resources Information Center
Building E38-320
MIT
Cambridge, MA 02139

Library
Lamont-Doherty Geological Observatory
Columbia University
Palisades, NY 10964

Library
Serials Department
Oregon State University
Corvallis, OR 97331

Pell Marine Science Library
University of Rhode Island
Narragansett Bay Campus
Narragansett, RI 02882

Working Collection
Texas A&M University
Dept. of Oceanography
College Station, TX 77843

Fisheries-Oceanography Library
151 Oceanography Teaching Bldg.
University of Washington
Seattle, WA 98195

Library
R.S.M.A.S.
University of Miami
4600 Rickenbacker Causeway
Miami, FL 33149

Maury Oceanographic Library
Naval Oceanographic Office
Building 1003 South
1002 Balch Blvd.
Stennis Space Center, MS, 39522-5001

Library
Institute of Ocean Sciences
P.O. Box 6000
Sidney, B.C. V8L 4B2
CANADA

National Oceanographic Library
Southampton Oceanography Centre
European Way
Southampton SO14 3ZH
UK

The Librarian
CSIRO Marine Laboratories
G.P.O. Box 1538
Hobart, Tasmania
AUSTRALIA 7001

Library
Proudman Oceanographic Laboratory
Bidston Observatory
Birkenhead
Merseyside L43 7 RA
UNITED KINGDOM

IFREMER
Centre de Brest
Service Documentation - Publications
BP 70 29280 PLOUZANE
FRANCE

50272-101

REPORT DOCUMENTATION PAGE	1. REPORT NO. WHOI-2002-01	2.	3. Recipient's Accession No.

4. Title and Subtitle
Shearmeter Floats in the Area of the WHOI Brazil Basin Tracer Release Experiment: Technical and Oceanographic Data

5. Report Date
January 2002

6.

7. Author(s) Timothy F. Duda, Brian J. Guest, Christine M. Wooding, Clayton M. Jones, Scott Lelievre and Douglas C. Webb

8. Performing Organization Rept. No.
WHOI-2002-01

9. Performing Organization Name and Address

Woods Hole Oceanographic Institution
Woods Hole, Massachusetts 02543

10. Project/Task/Work Unit No.

11. Contract(C) or Grant(G) No.
(C) OCE-9416014
(G) OCE-9906685

12. Sponsoring Organization Name and Address

National Science Foundation

13. Type of Report & Period Covered
Technical Report

14.

15. Supplementary Notes
This report should be cited as: Woods Hole Oceanog. Inst. Tech. Rept., WHOI-2002-01.

16. Abstract (Limit: 200 words)

Six drifting floats designed to measure shear were deployed in the vicinity of the Brazil Basin Tracer Release Experiment. The one-year long time series of oceanographic conditions obtained by the floats are for direct comparison with long-term tracer dispersion. The purpose of the tracer dispersion experiment was to study mixing of Antarctic Bottom Water at approximately 4000 m depth with less dense water above. Two of the floats returned shear records, one from about 1660 m depth and one from about 2800 m depth. Mean shear at 1660 m was 2.2 x 10 -3 s-1 with N = 1.1 cph, about 1.9 times the Garrett-Munk model amount. Mean shear at 2800 m was 1.1 x 10-3 with N = 0.5 cph, about 2.2 times Garrett-Munk. There was no apparent depth structure to the shear recorded by the near-bottom float moving over the mountainous seafloor. The two shear time series and the local tidal velocities were not strongly correlated, but the tide and shear series did have some similarities. Some variability in the 1660-m shear may be due to atmospheric forcing. Three floats deeper than 2800 m returned one-year long trajectories. Two trajectories were persistently eastward.

17. Document Analysis **a. Descriptors**
Shear
abyssal currents
finestructure

b. Identifiers/Open-Ended Terms

c. COSATI Field/Group

18. Availability Statement
Approved for public release; distribution unlimited.

19. Security Class (This Report)
UNCLASSIFIED

20. Security Class (This Page)

21. No. of Pages
44

22. Price

(See ANSI-Z39.18) *See Instructions on Reverse*

OPTIONAL FORM 272 (4-77)
(Formerly NTIS-35)
Department of Commerce